ISSN 1063-7745, Crystallography Reports, 2016, Vol. 61, No. 6, pp. 954–973. © Pleiades Publishing, Inc., 2016.
Original Russian Text © I.I. Prokofev, A.A. Lashkov, A.G. Gabdulkhakov, V.V. Balaev, T.A. Seregina, A.S. Mironov, C. Betzel, A.M. Mikhailov, 2016, published in Kristallografiya, 2016, Vol. 61, No. 6, pp. 919–939.

STRUCTURE OF MACROMOLECULAR COMPOUNDS

X-Ray Structures of Uridine Phosphorylase from *Vibrio cholerae* in Complexes with Uridine, Thymidine, Uracil, Thymine, and Phosphate Anion: Substrate Specificity of Bacterial Uridine Phosphorylases

I. I. Prokofev[a], A. A. Lashkov[a,*], A. G. Gabdulkhakov[a], V. V. Balaev[a], T. A. Seregina[a], A. S. Mironov[b], C. Betzel[c], and A. M. Mikhailov[a]

[a] *Shubnikov Institute of Crystallography of Federal Scientific Research Centre "Crystallography and Photonics", Russian Academy of Sciences, Moscow, 119333 Russia*

[b] *State Research Institute of Genetics and Selection of Industrial Microorganisms, Moscow, 117545 Russia*

[c] *University of Hamburg, Mittelweg 177, Hamburg, 20148 Germany*

** e-mail: alashkov83@gmail.com*

Received May 26, 2016

Abstract—In many types of human tumor cells and infectious agents, the demand for pyrimidine nitrogen bases increases during the development of the disease, thus increasing the role of the enzyme uridine phosphorylase in metabolic processes. The rational use of uridine phosphorylase and its ligands in pharmaceutical and biotechnology industries requires knowledge of the structural basis for the substrate specificity of the target enzyme. This paper summarizes the results of the systematic study of the three-dimensional structure of uridine phosphorylase from the pathogenic bacterium *Vibrio cholerae* in complexes with substrates of enzymatic reactions—uridine, phosphate anion, thymidine, uracil, and thymine. These data, supplemented with the results of molecular modeling, were used to consider in detail the structural basis for the substrate specificity of uridine phosphorylases. It was shown for the first time that the formation of a hydrogen-bond network between the 2'-hydroxy group of uridine and atoms of the active-site residues of uridine phosphorylase leads to conformational changes of the ribose moiety of uridine, resulting in an increase in the reactivity of uridine compared to thymidine. Since the binding of thymidine to residues of uridine phosphorylase causes a smaller local strain of the β-N1-glycosidic bond in this the substrate compared to the uridine molecule, the β-N1-glycosidic bond in thymidine is more stable and less reactive than that in uridine. It was shown for the first time that the phosphate anion, which is the second substrate bound at the active site, interacts simultaneously with the residues of the β5-strand and the β1-strand through hydrogen bonding, thus securing the gate loop in a conformation so that the active site of the enzyme molecule becomes inaccessible for nucleoside binding.

DOI: 10.1134/S1063774516060134

INTRODUCTION

Uridine phosphorylase (UPh, EC 2.4.2.3) [1–4] catalyzes the reversible phosphorolytic cleavage of uridine and, less efficiently, of thymidine to nitrogenous bases [5]. In many types of human tumor cells and infectious agents, the demand for pyrimidine nitrogen bases increases during the development of the disease, thus raising UPh expression levels [6–10]. This is evidence of the importance of uridine phosphorylase in metabolic processes. The three-dimensional structures of the binding sites of UPhs from different sources are highly conserved, and the reaction catalyzed by this enzyme has a common mechanism.

Uridine phosphorylase and its ligands, in particular, substrates and inhibitors, are of interest for pharmaceutical and biotechnology industries. Their rational use requires knowledge of the structural basis for the substrate specificity of the target enzyme. Human uridine phosphorylases (*h*UPP1 and *h*UPP2) [11–15] are involved in the activation of antitumor agents, for example, capecitabine, a triple prodrug of 5-fluorouracil [16]. By considering enzyme–substrate specificity, prodrugs can be designed to target tumor cells, where they are selectively activated by *h*UPP1 or *h*UPP2, in order to reduce the side effects on neighboring normal (healthy) cells [16]. It is also necessary to take into account the substrate specificity of UPh in the design of antibacterial and antiparasitic (in particular, against *Giardia intestinalis* and *Schistosoma mansoni* [17–19]) drugs of a nucleoside nature metabolized by UPh. For instance, it is possible to predict the

Table 1. Expression of the *Vch*UPh gene

Gene source organism	*Vibrio cholerae* O1 biovar El Tor (strain ATCC 39315 / El Tor Inaba N16961)
DNA source	*Vibrio cholerae*
Forward primer*	5'-CCG*GATCC*GCGCCACATCAAGTGGCGC-3'
Reverse primer*	5'-GGG*GAATTC*AAGTAGGAAGGGGATAGAGG-3'
Cloning vector	pUC19
Expression vector	pUC19
Producer organism	*Escherichia coli*
Amino acid sequence of the final enzyme	MTKTVFHLGVTEADLNGATLAIIPGDPARVQKIAELMDNPVFLASHREYTVYRAEL DGQSVVVCSTGIGGPSTSIAVEELAQLGVRTFLRVGTTGAIQPHVNVGDMIVTTGSV RLDGASLHFAPMEFPAVPDFDVATAMKAAAQESGATVHMGVTASSDTFYPGQERY DTFTGRVVRRFQGSMKEWQDMGVLNFEMESATLLTMCASSGLKAGCVAGVIINRT QKEIPDHATLKETEARSIKVVVEAARKMLK

* The nucleotide recognition sequence for restriction enzymes is underlined.

influence of modifications of the 2'-hydroxy and 5-methyl groups of the ligands on the pharmacokinetics and pharmacodynamics of potential drugs.

Knowledge of the structural basis for the substrate specificity of UPh is also important for performing modifications of the enzyme by genetic engineering for the subsequent use of UPh in the industrial enzymatic synthesis of biologically active nucleosides (for example, arabinofuranosyl nucleosides) [20].

Despite the above-discussed importance of research on the structural basis for the substrate specificity of UPh, systematic investigations into the structures of the enzyme in complexes with substrates of the forward (nucleoside phosphorolysis) and reverse (nucleoside synthesis) reactions are lacking. The structures of a number of complexes of bacterial UPhs with substrates of the forward and reverse reactions, some of which were determined at insufficiently high resolution, are available in the literature [5]. In [5] the higher efficiency of the enzyme toward uridine than to thymidine was attributed to the presence of three additional hydrogen bonds between the 2'-hydroxy group of uridine and the residues of the ribose-binding site of bacterial uridine phosphorylase from *E. coli* (*Ec*UPh). In [20] the biochemical constants K_{cat}, K_M, and K_{cat}/K_M for the *Ec*UPh-catalyzed reactions with natural and synthetic nucleosides were determined, and it was shown that the 5-methyl group of the substrate also influences, although to a lesser degree than the 2'-hydroxy group, the rate of the chemical reaction.

In the present work, we performed the first systematic study of uridine phosphorylase from the pathogenic bacterium *Vibrio cholerae* (*Vch*UPh) in complexes with substrates of the forward and reverse reactions—uridine, phosphate anion, thymidine, uracil, and thymine (ID PDB: 5C80, 4IP0, 4LZW, 4OEH, 4OGL, respectively)—in the crystalline state. These data, supplemented with the results of molecular modeling, allowed us to consider in detail the structural basis for the substrate specificity of UPh toward both the natural substrates of the forward phosphorolysis reaction (uridine, thymidine, and phosphate anion) and substrates of the reverse reaction (uracil and thymine).

MATERIALS AND METHODS

Isolation and Purification of VchUPh

Procedures for the production of the biomass and for the isolation and purification of the *Vch*UPh enzyme have been described in detail earlier [21–23] (Table 1).

A highly homogeneous solution of *Vch*UPh was obtained by chromatography on a column packed with butyl sepharose in the first stage and on a column with *Q*-sepharose in the final stage. The final purity of *Vch*UPh was ~96%, as estimated by gel electrophoresis under denaturing conditions using sodium dodecyl sulfate on 15% polyacrylamide gel (PAG).

The homogeneity of the protein sample assessed by gel electrophoresis under nondenaturing conditions on 7.5% PAG was 98%. The enzyme *Ec*UPh, which has a similar mobility, was used as the marker.

Crystallization

The screening of crystallization conditions for the complexes was performed using the Classics, MbClass, and MbClass II Suites (QIAGEN, www.qiagen.com) crystallization kits.

The crystallization of the complexes was carried out by the vapor-diffusion technique at 291 K. The crystals of *Vch*UPh in complexes with ligands suitable for X-ray diffraction appeared within 1 week. The crystallization drops were composed of 1.5 μL of a *Vch*UPh solution with a protein concentration of 15 mg/mL in Tris-HCl buffer, 1.5 μL of the reservoir solution, and 1 μL of an aqueous solution of the ligand. The molar concentrations of the ligand solutions are given in Table 2.

Table 2. Crystallization of *Vch*UPh complexes

	With thymidine	With uridine	With uracil	With thymine	With phosphate anion
Crystallization method	Hanging-drop vapor-diffusion				Sitting-drop vapor-diffusion
Composition of the protein solution	20 mM Tris-HCl, pH 7.5, 20 mM NaCl				
Composition of the reservoir solution	0.2 *M* $MgCl_2 \cdot 6H_2O$, 15% (w/v) PEG 4000, 0.1 *M* Tris-HCl, pH 8.5				0.5 M sodium diphosphate; 0.1 M ammonium sulfate, 0.5 M potassium diphosphate, pH 7.5
Drop volume and ratio	2 μL of protein solution, 2 μL of reservoir solution, and 1 μL of 0.1 M thymidine	2 μL of protein solution, 2 μL of reservoir solution, and 1 μL of 0.1 M uridine	2 μL of protein solution, 2 μL of reservoir solution, and 1 μL of 0.2 M uracil	2 μL of protein solution, 2 μL of reservoir solution, and 1 μL of 0.2 M thymine	1 μL of protein solution, 1 μL of reservoir solution
Volume of the reservoir solution	300 μL				

X-ray Diffraction Data Collection

The experimental X-ray diffraction data sets were collected from crystals of *Vch*UPh in complexes with uracil and thymine at the macromolecular crystallography beamline P11 at the synchrotron source PETRA III (DESY, Hamburg, Germany), from crystals of *Vch*UPh in complexes with thymidine and phosphate anion at the beamline X13 at the DORIS synchrotron radiation storage ring (DESY/EMBL, Hamburg, Germany), and from crystals of *Vch*UPh in complex with uridine at the beamline 14.1 at the BESSY II synchrotron radiation source (Helmholtz-Zentrum, Berlin, Germany). The X-ray diffraction data sets were measured at 100 K. Before exposure to X-rays, the crystals were soaked in a cryoprotectant solution for 5 s composed of the reservoir solution supplemented with 40% glycerol. The X-ray data collection statistics are given in Table 3.

The experimental X-ray diffraction intensities were processed using the XDS program [24]. The X-ray data processing statistics for all five complexes of *Vch*UPh with the ligands are given in Table 3. The intensities were scaled and the structure factor magnitudes were calculated using the SCALA program [25].

Structure Solution and Refinement

The initial phases of the structure factors for the solution of the three-dimensional structures of *Vch*UPh in complexes with phosphate anion, uridine, uracil, and thymine were obtained by the molecular-replacement method using the Molrep program [26]; for the structure of the *Vch*UPh in complex with thymidine they were obtained using the Phaser program [27]. The structure of *Vch*UPh in complex with thymidine was solved using the structure of unligated *Vch*UPh at 1.7 Å resolution (ID PDB: 3O6V) as the starting model. In all other cases, the structure of *Vch*UPh in complex with thymidine at 1.29 Å resolution (ID PDB: 4LZW) served as the starting model. The atoms of all ligands, including bound water molecules, were removed from all starting structures.

The structures of *Vch*UPh in complexes with the ligands were refined using the *phenix.refine* [28] and REFMAC program packages [29]. For the complexes of *Vch*UPh with thymidine, thymine, and phosphate anion, all atom displacement parameters were refined anisotropically; for *Vch*UPh in complexes with uracil and uridine they were refined isotropically. The automatic structure-refinement cycles were alternated with manual rebuilding in the interactive graphics program Coot [30, 31]. The atoms of the ligands and water molecules were located in σ_A-weighted Fourier electron-density maps calculated with the mF_o-DF_c and $2mF_o-DF_c$ coefficients.

The validity of the structure refinement was checked with the PROCHECK program [32] and the MolProbity web service [33]. The principal structure-refinement statistics are given in Table 4. The figures were drawn with the PyMol program [34]. The amino-acid sequence alignment was performed using the ClustalW2 software [35]. The secondary-structure elements were extracted in the ESPript 3.0 server [36]. The schematic diagram of enzyme–substrate interactions was generated with the LIGPLOT program [37]. The structures were deposited in the Research Collaboratory for Structural Bioinformatics Protein Data Bank (RCSB-PDB). The ID PDB (http://www.rcsb.org/) are listed in Table 4.

Table 3. X-ray data-collection and processing statistics for *Vch*UPh complexes*

	With thymidine	With uridine	With uracil	With thymine	With phosphate anion
Wavelength, Å	0.81	0.98	1.00	1.00	0.81
Detector	MAR CCD 165 mm	PSI pilatus 6M	PSI pilatus 6M	PSI pilatus 6M	MAR CCD 165 mm
Crystal-to-detector distance, mm	71.38	394.80	380.00	156.61	180.69
Rotation step, deg	0.5	0.1	0.2	0.2	0.5
Total rotation range, deg			360		
Exposure time, s	30	1	1	1	30
Sp. gr.	$P2_1$	$P1$	$P1$	$P2_1$	$P1$
Number of molecules per asymmetric unit			1		
a, b, c, Å	91.74, 95.85, 91.83	61.26, 73.11, 83.14	64.26, 71.76, 89.32	92.75, 96.50, 92.78	63.67, 71.06, 87.91
α, β, γ, deg	90, 119.96, 90	71.81, 77.19, 85.69	69.14, 72.15, 85.79	90, 119.99, 90	69.63, 72.56, 85.73
Mosaicity, deg	0.19	0.55	0.28	0.09	0.14
Resolution range, Å	29.65–1.29 (1.34–1.29)	77.23–2.24 (2.36–2.24)	79.60–1.91 (2.01–1.91)	41.81–1.25 (1.32–1.25)	78.79–1.29 (1.36–1.29)
Total number of reflections	1435540 (153760)	101646 (13271)	185700 (27074)	786665 (330285)	1254860 (127989)
Number of unique eflections	345305 (36724)	58293 (7810)	104334 (15043)	383390 (54747)	327958 (47257)
Completeness, %	99.2 (99.1)	91.1 (83.2)	94.4 (92.8)	98.3 (96.5)	95.5 (94.3)
Redundancy	2.3 (2.3)	1.7 (1.7)	1.8 (1.8)	6.7 (6.0)	3.8 (2.7)
Average value $\langle I/\sigma(I)\rangle$	9.3 (2.0)	9.6 (2.3)	9.0 (1.9)	17.0 (2.7)	14.2 (2.3)
Overall Wilson temperature factor, Å^2	14.59	43.51	21.01	10.56	14.22

* The data for the last high-resolution shell are given in parentheses.

Calculations of Partial Electric Charges on Atoms in Uridine and 5-Methyluridine Molecules

In order to reveal the changes in the physicochemical properties of the ligands depending on their structure and find the relationship between these properties and the selectivity of the enzyme, we calculated the partial electric charges on atoms. The effect of the 5-methyl group on the intramolecular charge distribution was examined by performing calculations with the use of 5-methyluridine as an analog of thymidine instead of thymidine by itself, due to which there was no need to take into account the absence of the 2′-hydroxy group in the thymidine molecule, which is present in uridine.

The partial electric charges on atoms of the 5-methyluridine and uridine ligands, as well as of the thymine and uracil molecules, were calculated with the Jaguar 7.9 suite of programs [38] in a water environment at the Hartree–Fock level of theory with the 3-21G basis set. All other calculation parameters were set to the default values recommended by the Jaguar 7.9 program authors.

Calculations of the Conformational Energy of Thymidine, Uridine, Ribose 1-Phosphate, and 2-Deoxyribose 1-Phosphate Molecules in Complexes with VchUPh and in Aqueous Solution

The conformational energies of the ligand molecules in solution and in complexes with *Vch*UPh were calculated with the MacroModel program [39] using the OPLS-2005 force field [40] with an implicit solvent model. A conformational search for ligands in solution was performed with the Minimization module implemented in this program using the following energy-minimization parameters: the maximum number of iterations was 2000, the convergence threshold was 0.05 kJ/mol, and the Polak–Ribier conjugate gradient (PRCG) minimization algorithm [41]. In order to analyze the energy, which is independent of direct interactions between the ligands and atoms of the protein or water environment, we calculated the value of E':

$$E' = E_{\text{stretch}} + E_{\text{bend}} + E_{\text{tors}} + E_{\text{tors\_improper}},$$

where E_{stretch} is the energy associated with stretching or compression of valence bonds, E_{bend} is the energy

Table 4. Structure-solution and refinement statistics for *Vch*UPh complexes

	With thymidine	With uridine	With uracil	With thymine	With phosphate anion
Resolution range, Å	19.89–1.29 (1.30–1.29)	45.47–2.24 (2.30–2.24)	44.27–1.91 (1.96–1.91)	7.99–1.25 (1.26–1.25)	18.93–1.29 (1.31–1.29)
Completeness, %	99.3	90.9	94.4	98.2	94.7
Cutoff Sigma, σ(|F|)	$F > 2.0\sigma(F)$	$F > 0.0\sigma(F)$	$F > 0.0\sigma(F)$	$F > 0.0\sigma(F)$	$F > 2.0\sigma(F)$
Number of reflections in the working set	342140 (10708)	55318 (3297)	99133 (7111)	381769 (11734)	324967 (9339)
Number of reflections in the test set	17105 (563)	2849 (173)	5198 (397)	19179 (648)	16457 (520)
R_{work}	0.178 (0.255)	0.168 (0.278)	0.172 (0.293)	0.115 (0.200)	0.172 (0.431)
R_{free}	0.211 (0.285)	0.237 (0.337)	0.216 (0.329)	0.147 (0.240)	0.200 (0.482)
Cruickshank DPI, Å	0.06	0.59	0.12	0.04	0.06
Number of refined non-hydrogen atoms					
Protein	11192	11318	11258	11243	11257
Ions	18	8	3	3	5
Ligands	131	260	106	134	81
Water	1967	822	1275	2169	1998
Rmsd from ideal geometry					
Bond lengths, Å	0.014	0.009	0.007	0.008	0.008
Bond angles, deg	1.324	1.532	1.154	1.273	1.216
Average *B* factor for atoms, Å^2					
Protein	10.1	30.6	22.8	15.6	9.6
Ions	14.9	45.1	29.3	14.7	23.2
Ligands	12.0	25.1	30.0	22.4	28.1
Water	24.7	37.7	30.3	31.7	23.6
Ramachandran statistics					
Number of residues in the most favored regions, %	98.79	97.33	98.39	98.46	98.79
Number of residues in the allowed regions, %	1.44	2.27	1.21	1.19	0.81
ID PDB	4LZW	5C80	4OEH	4OGL	4IP0

* The data for the last high-resolution shell are given in parentheses.

required for bending the bond angles, E_{tors} is the energy of torsion angles, and $E_{tors\_improper}$ is the improper torsion energy.

Molecular Docking and Geometry Optimization

The structures of *Vch*UPh in complexes with thymine and uracil were prepared for molecular docking of the second substrates of the reverse reaction (ribose 1-phosphate and 2-deoxyribose 1-phosphate) using the Protein Preparation Wizard available in the Maestro suite (Schrödinger Release 2014-4: Maestro, version 10.0, Schrödinger, LLC, New York, 2014). The preparation included the addition of coordinates of missing hydrogen atoms and calculations of the partial atomic charges. The stereochemical data on the structures of ribose 1-phosphate and 2-deoxyribose 1-phosphate were extracted from the PubChem Database [42]. The geometry optimization of the ligand molecules was performed with the PRODRG web service [43]. The molecular docking was carried out with the Glide docking tool available in the Maestro program suite (Extra Prescription Glide, which implies the mobile ligand and the stationary target) [44]. The docking results were ranked using the Glide Score docking scoring function [44].

For the geometry optimization of the structures obtained by docking simulations, the atomic characteristics were parameterized using the GROMACS/GMX all-atom force field [45]. The models of the protein complexes were placed in a virtual rectangular-paral-

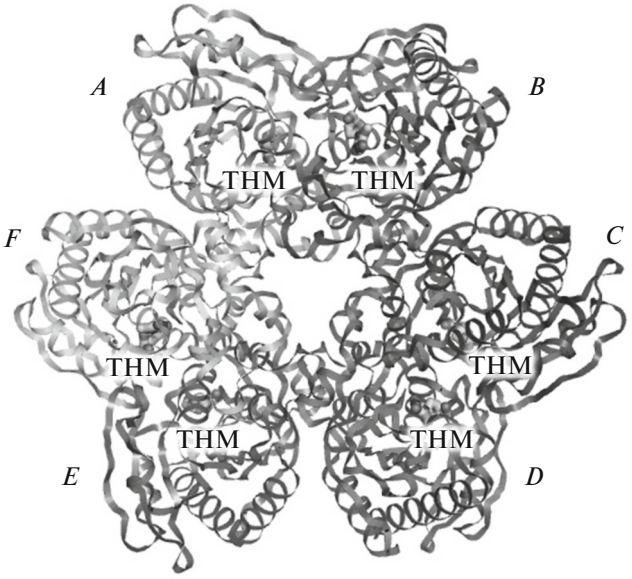

Fig. 1. Quaternary structure of the enzyme *Vch*UPh in complex with thymidine.

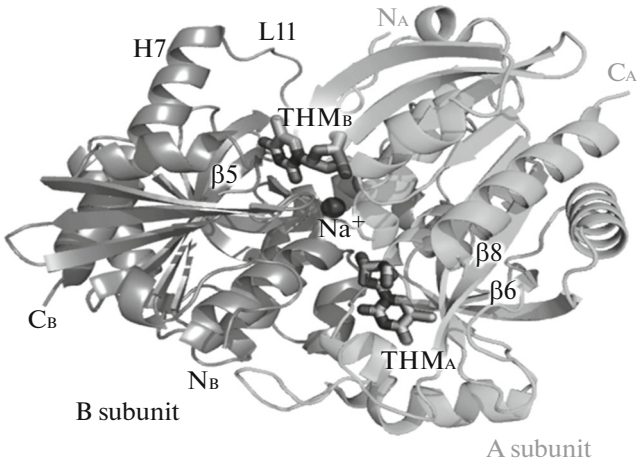

Fig. 2. Spatial organization of the AB homodimer of the *Vch*UPh complex containing thymidine (THM) at the enzyme active site and a sodium ion (Na+) at the intersubunit interface. The N- and C-termini are labeled by the letters N and C, respectively. The secondary-structure elements, which are mentioned in the text below, are denoted.

lelepiped-shaped cell with dimensions of 80 × 70 × 75 Å. The minimum distance between the atomic coordinates of the protein and the face of the cell is 9 Å. The atomic characteristics of water molecules were parameterized and the distribution of water molecules within the virtual cell environment was carried out with the genbox program (GROMACS [45]) using the SPC216 three-site water model. The overall charge of the system was compensated for by adding sodium ions to the models. The geometry optimization was performed with the GROMACS software package using the following parameters: the integration step was 0.001 ps, the number of integration steps was 10000, the Ewald summation for calculating electrostatic interactions.

RESULTS AND DISCUSSION

Structural Organization of VchUPh

The quaternary structure of the *Vch*UPh complexes under consideration is a hexamer (Fig. 1) composed of six homologous subunits. The outer diameter of the toroidal hexamer is ~106 Å.

The hexameric structure of *Vch*UPh in complexes with ligands is stabilized by van der Waals and hydrophobic interactions and hydrogen bonds between residues of adjacent homodimers. In addition to inter-homodimer contacts between adjacent subunits, the enzyme molecule is stabilized by hydrogen bonds between the subunits related by a threefold axis.

The surface area of the inter-homodimer interface in the *Vch*UPh molecule is 1017 Å^2, and the free energy of solvation is −20.4 kcal/mol (PDBePISA [46]).

Each homodimer of *Vch*UPh in complexes with the ligands is stabilized by van der Waals interactions, hydrophobic interactions, and hydrogen and ionic bonds.

The surface area of the intersubunit interface taking into account the sodium ion that is present in the homodimer is 1905 Å^2, and the free energy of solvation estimated with the PDBePISA server [46] is −20.2 kcal/mol. The latter value is larger in magnitude that the free energy of solvation for *Salmonella typhimurium* uridine phosphorylase (*St*UPh) (ID PDB: 3DPS) (−15.6 kcal/mol), which we have studied earlier [47, 48].

Tertiary, Secondary, and Primary Structures of VchUPh Complexes

The arrangement of the secondary-structure elements of the subunit can be classified as a three-layer αβα sandwich Rossmann fold [49] (Fig. 2). The monomer of the enzyme molecule consists of eight β strands, which form three β-sheets, surrounded by eight α helices.

The secondary structure of the *Vch*UPh molecule in the complexes includes 32% of α helices and 28% of β strands (Fig. 3). The subunit of the hexameric *Vch*UPh molecule has a molecular weight of 27.5 kDa [23] and is composed of 253 residues. Hydrophobic residues are distributed throughout the subunit and play a key role in the formation of the structural core of the molecule.

In all the complexes under consideration, a Na^+ ion is present at the intersubunit interface of each homodimer of the hexameric molecule. In the complex of *Vch*UPh with thymidine (ID PDB: 4LZW) (Fig. 2), the sodium ion is coordinated by the side-chain atoms of the residues Glu48 and Ser72 and the carbonyl oxygen atom of Ile68 of one *Vch*UPh subunit

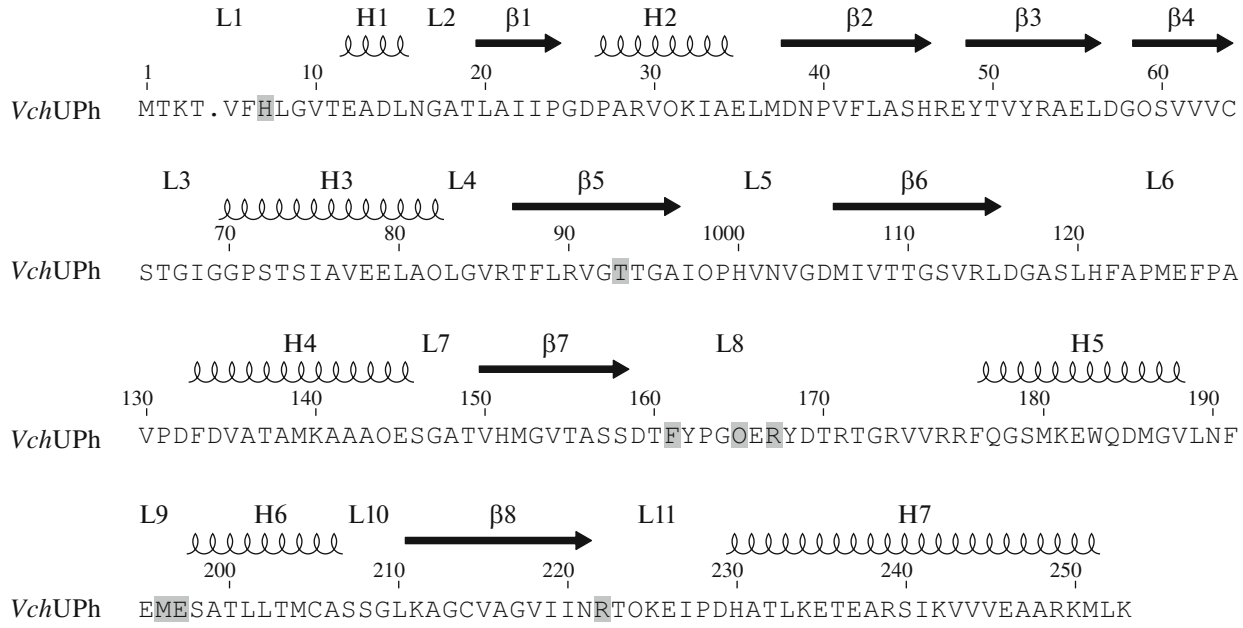

Fig. 3. Primary amino-acid sequence and the secondary structure of *Vch*UPh. Active-site residues of the enzyme are highlighted.

and the corresponding symmetry-related (pseudo-twofold axis) residues of the adjacent subunit of the homodimer. The oxygen atoms of the residues involved in the coordination of the Na^+ ions occupy the vertices of a distorted octahedron.

In the structure of *Vch*UPh complexed with thymidine, the distances from the Na^+ ion to the atoms of the nearest residues (in the AB dimer) are as follows: Na^+—2.80 Å—OE2_Glu48/B, Na^+—2.95 Å—O_Ile68/B, Na^+—2.88 Å—OG_Ser72/B, Na^+—2.79 Å—OE2_Glu48/A, Na^+—2.98 Å—O_Ile68/A, Na^+—2.90 Å—OG_Ser72/A. Identical contacts are observed between the sodium ion and the atoms of the amino-acid residues in the *Vch*UPh complexes with uracil, uridine, phosphate anion, and thymine.

The structures of bacterial UPhs containing a K^+ ion at the intersubunit interface were described in [5, 48]. In order to compare the positions of the Na^+ and K^+ ions in the structures and assess their effect on the conformations of the residues in the enzyme, we superimposed the secondary-structure elements of *St*UPh in complex with 2.2'-anhydrouridine (ID PDB: 3FWP; [48]) and of *Vch*UPh in complex with thymidine (ID PDB: 4LZW). The residues bound to the Na^+ ion are completely identical to those bound to the K^+ ion. The distance between the K^+ and Na^+ ions in the superimposed structures (ID PDB: 3FWP and 4LZW) is 0.180 Å, and the rms deviation between the atomic coordinates of the residues bound to the ions (Glu48/E, Glu48/F, Ser72/E, Ser72/F, Ile68/E, Ile68/F in *Vch*UPh complexed with thymidine and the corresponding residues in *St*UPh) is 0.484 Å. This comparison demonstrates the similar spatial arrangement of the residues in the vicinity of the ions (Na^+ or K^+) in these two enzymes.

Binding Sites in VchUPh

Each homodimer of the *Vch*UPh molecule contains two identical enzyme active sites located in canyons at the intersubunit interface of the enzyme homodimer (Fig. 2). The entries to the active sites of the adjacent subunits of the homodimer lie on the opposite sides of the equatorial plane of the hexamer and are spaced by 20 Å. The active site consists of the phosphate- and nucleoside-binding sites. The latter site is subdivided into the uracil- and ribose-binding subsites. The substrate-binding sites are formed by residues of both subunits of the homodimer (Fig. 2). Hereinafter, the binding sites are labeled with the same letters as the subunits of the homodimer, which provide a larger number of residues for the formation of the appropriate binding site.

Phosphate-Binding Site

A phosphate anion was found with full occupancy at the phosphate-binding sites of the B, C, and F subunits of the *Vch*UPh complex (ID PDB: 4IP0). In this structure the active site of the E subunit contains a sulfate anion. The phosphate-binding sites of the A and D subunits in this structure are fully unligated.

The phosphate-binding F site of the EF homodimer of *Vch*UPh is formed by hydrophilic residues, four of which belong to the F subunit (Thr93/F, Gly25/F Arg29/F, and Arg90/F), and the fifth residue (Arg47/E) belongs to the E subunit (Fig. 4a). In the *Vch*UPh complex with the phosphate anion (ID PDB: 4IP0), the latter is bound to atoms of the phosphate-

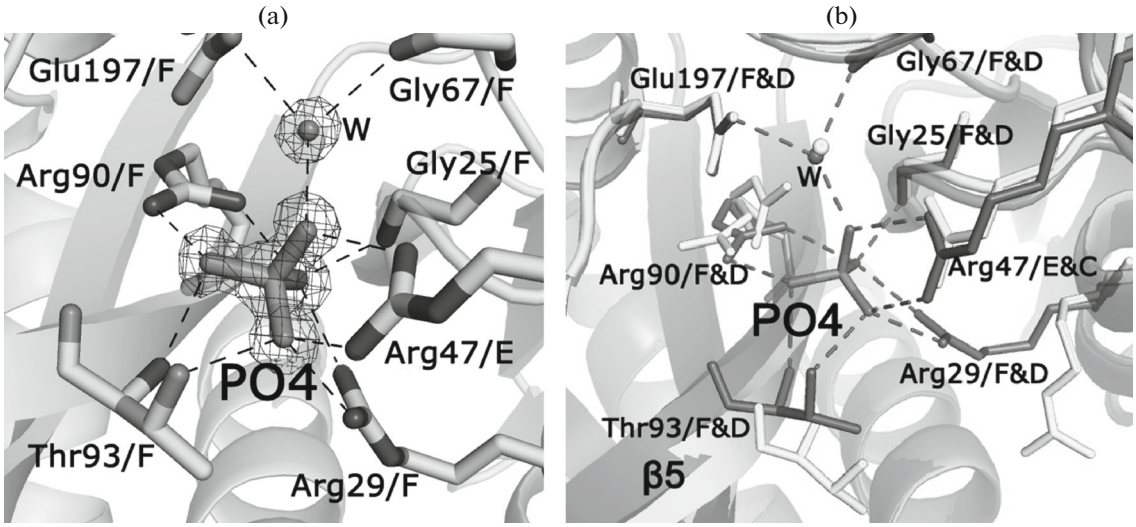

Fig. 4. (a) Spatial organization of the phosphate-binding pocket of the active site of *Vch*UPh in complex with a phosphate anion (ID PDB: 4IP0). The 2mFo-DFc electron density map is contoured at the 1.5 σ level. (b) The superposition of the phosphate-binding pocket and the β5 strand in the free state (white) and in the enzyme ligated (dark gray) with a phosphate anion (PO4).

binding F site (Fig. 4a) through the following hydrogen bonds: O3_PO4/F—2.76 Å—NH2_Arg90/F; O4_PO4/F—2.99 Å—NH1_Arg90/F; O2_PO4/F—2.67 Å—OG1_Thr93/F; O3_PO4/F—2.88 Å—N_Thr93/F; O3_PO4/F—3.17 Å—OG1_Thr93/F; O2_PO4/F—2.84 Å—NH2_Arg47/E; O1_PO4/F—2.86 Å—NH1_Arg47/E; O2_PO4/F—2.71 Å—NH2_Arg29/F; O4_PO4/F—2.79 Å— NH1_Arg29/F; O4_PO4/F—2.82 Å –N_Gly25/F.

In addition, the phosphate anion is bound through a structural water molecule to Gly67/F and Glu197/F by the following hydrogen bonds: O1_PO4/F—2.58 Å —H_2O—2.84 Å—O_Gly67/F; O1_PO4/F—2.58 Å—H_2O—2.83 Å—OE2_Glu197/F (Fig. 4a). In the structure of *Vch*UPh complexed with phosphate anion (ID PDB: 4IP0), the phosphate-binding sites of the A, D, and E subunits are either unligated or occupied by nonspecific ligands—glycerol or tris(hydroxymethyl)aminomethane (Tris) molecules.

The rms deviations (rmsd) between the atomic coordinates of the phosphate-binding-site residues of the F subunit of *Vch*UPh ligated by the phosphate anion and of the D subunit lacking the ion in the binding site is 1.6 Å. The maximum rms deviation between the atomic coordinates of the phosphate-binding site is observed for the side chain of Arg29/D (4.1 Å). In the binding site lacking the phosphate anion, Arg29/D forms a hydrogen bond with the main-chain carboxyl oxygen atom of Glu237/D: O_Glu237/D—2.92 Å—NH2_Arg29/D. The side-chain conformation of Arg29/D undergoes substantial changes upon the binding of the phosphate anion to the enzyme. Conformational changes are also observed for the side chains of Arg47/C and Arg90/D (Fig. 4b). The rms deviation between the atomic coordinates of the side chains of Arg47/E and Arg47/C is 0.699 Å; that of the side groups of Arg90/F and Arg90/D, 1.535 Å.

The rms deviation between the coordinates of the Cα atoms of the phosphate-binding-site residues of *Vch*UPh ligated by the phosphate anion (F) and of the residues involved in the unligated binding site (D) is 0.6 Å. The binding of the phosphate anion induces a 1.3 Å displacement of Thr93 deeper in the active site accompanied by the displacement of the adjacent residues Gly92, Thr94, and Gly95, which form a labile β5 strand (Figs. 2, 3, 4b). The rms deviations between the coordinates of the Cα atoms of residues Gly92, Thr94, and Gly95 of the *Vch*UPh subunits, one of which is ligated by the phosphate anion (F) and another one is in the free state (D), are 1.3, 0.9, and 0.8 Å, respectively.

For the A and D subunits unligated by the phosphate anion, the rms deviation between the side-chain atoms of residues Arg29, Arg90, and Arg47 belonging to the adjacent subunit of the homodimer is 1.633 Å, whereas the rms deviation between the atomic coordinates of the side chains of the corresponding residues involved in the active sites of the F and C subunits ligated by the phosphate anion is 0.708 Å. Therefore, in the case of the unligated state of the phosphate-binding site, the conformations of Arg29, Arg90, Thr93, and Arg47 vary from one subunit to another, but these conformations differ from their conformations in the bound state. In different subunits, the phosphate anion stabilizes flexible phosphate-binding-site residues in one conformation.

Nucleoside-Binding Site

Residues Gln165, Arg167, and Arg222 play a key role in the binding of the pyrimidine moiety of the ligand (uridine, thymidine, uracil, and thymine) to

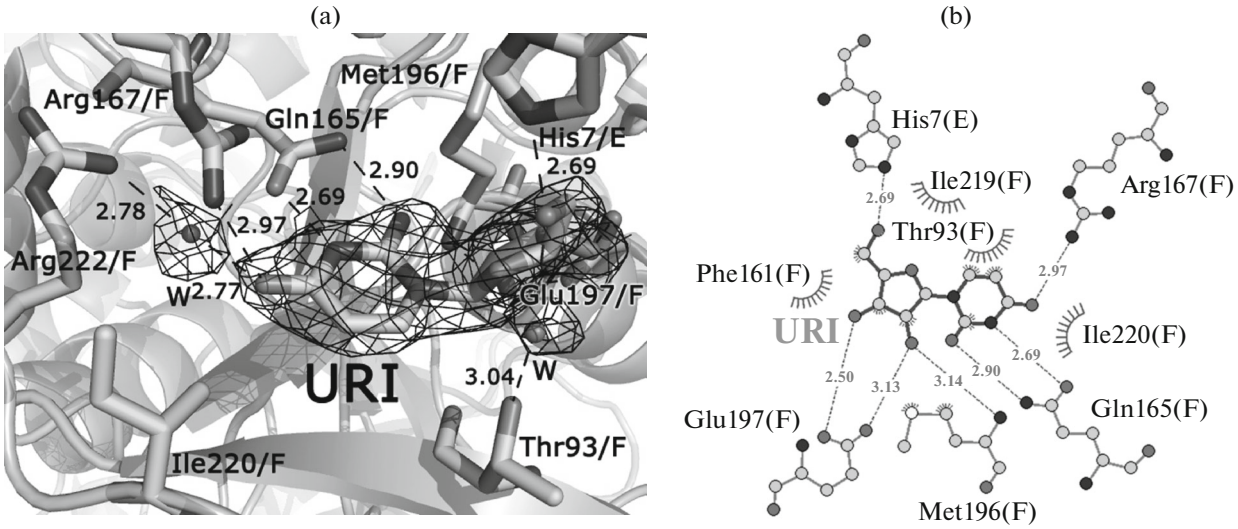

Fig. 5. (a) Active site of *Vch*UPh in complex with uridine URI (ID PDB: 5C80). The 2mFo-DFc electron density map is contoured at the 1.5 σ level. (b) The schematic diagram of enzyme–substrate interactions in the structure of *Vch*UPh complexed with uridine URI (ID PDB: 5C80).

*Vch*UPh (Figs. 5–9). Residues Glu197 and Thr93, as well as His7 of the adjacent subunit, play the main role in the binding of the furanose moiety of thymidine and uridine (Figs. 5, 6).

The phenyl group of Phe161 involved in the binding site is arranged perpendicular to the aromatic heterocycle of uridine, thymidine, uracil, or thymine and interacts with the latter via π stacking. A hydrophobic pocket formed by residues Ile220, Ile221, and Pro228, as well as by Phe8 of the adjacent subunit, is located in the vicinity of carbon atom C5 of the aromatic heterocycle of the ligands (uridine, thymidine, uracil, and thymine).

The uridine (URI) molecule occupies the whole nucleoside-binding site of the *Vch*UPh molecule (Fig. 5a). The URI molecule interacts with the nucleoside-binding site in the structure of *Vch*UPh complexed with uridine (ID PDB: 5C80) through hydrogen bonds: OE1_Gln165/F—2.69 Å—N3_URI; NE2_Gln165/F—2.90 Å—O2_URI; NH2_Arg167/F—2.97 Å—O4_URI; O4_URI—2.77 Å—H2O—2.78 Å—NH2_Arg222/F; NE2_His7/E—2.69 Å—O5'_URI; OE2_Glu197/F— 2.50 Å—O3′_URI; OE1_Glu197/F—3.13 Å— O3'_URI; OE1_Glu197/F—2.56 Å—O2′_URI; N_Met196/F—3.14 Å—O2'_URI; O5′_URI—2.85 Å—H2O—3.04 Å—OG1_Thr93/F.

The rms deviation between the atomic coordinates of the nucleoside-binding-site residues of the F subunit in *Vch*UPh complexed with uridine (ID PDB: 5C80) and of the unligated C subunit of *Vch*UPh complexed with uracil (ID PDB: 4OEH) is 0.964 Å. The atoms of Thr93 involved in the β5 strand make a major contribution to the above-given rmsd value (rmsd between the coordinates of the side-chain atoms of Thr93 is 3.235 Å; that of the main-chain atoms is 1.668 Å). After the exclusion of Thr93 from the calculation of rmsd, we obtained the value of 0.403 Å, which attests to a conformational similarity of the binding sites under consideration. Therefore, the URI molecule has only a slight effect on the configuration of the binding site, with the exception of Thr93 involved in the β5-strand.

Thymidine (THM) is present at all six active sites in the structure of the *Vch*UPh complex (ID PDB: 4LZW). The active sites of the A, B, D, and F subunits contain a ligand molecule with full occupancy; in the other two subunits (C and E), the ligand is present with partial occupancy. Like URI in the structure of *Vch*UPh complexed with uridine (ID PDB: 5C80), THM (ID PDB: 4LZW) interacts with the nucleoside-binding site of the biological *Vch*UPh molecule (see the F site of the EF dimer; ID PDB: 4LZW) through hydrogen bonds shown in Fig. 6.

In the active sites of the C and E subunits of *Vch*UPh in complex with THM (ID PDB: 4LZW), the occupancy factors for the THM molecule are 0.75 and 0.79, respectively. In these subunits, residues 92 and 93 involved in the β5 strand are disordered over two conformations (Figs. 3, 6, 7). In the E subunit, the displacements of the Cα and Cβ atoms in the alternative conformation of Thr93/E are 0.57 and 1.13 Å, respectively. The displacements of the Cα and Cβ atoms in the alternative conformation of Gly92/E are 0.27 and 0.90 Å, respectively. The rms deviation between the atomic coordinates of residues 92 and 93 in one of the two positions (position A) in the E subunit of *Vch*UPh complexed with thymidine and the corresponding residues of the A subunit in the structure of unligated *Vch*UPh (ID PDB: 3O6V, 1.70 Å resolution, DPI 0.09 Å) is 0.67 Å, whereas the rms deviation for the second position in the E subunit (position B) is 1.21 Å. The rms deviation between the atomic coordinates of residues 92 and 93 in one of the possible double posi-

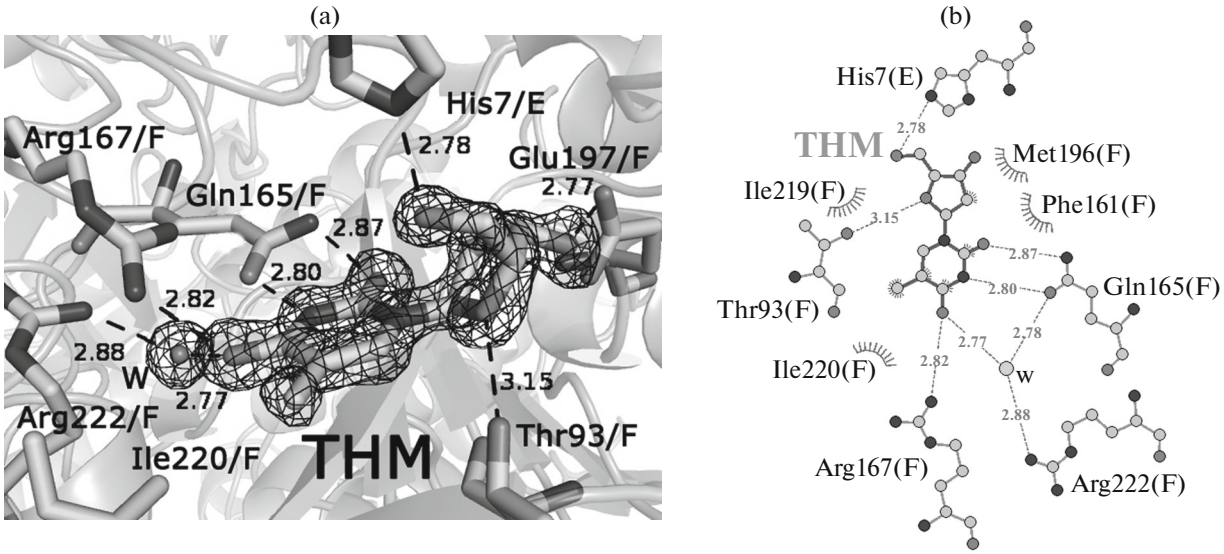

Fig. 6. (a) Active site of *Vch*UPh in complex with thymidine THM (ID PDB: 4LZW). The 2mFo-DFc electron density map is contoured at the 1.5 σ level. (b) The schematic diagram of enzyme–substrate interactions in the structure of *Vch*UPh complexed with thymidine THM (ID PDB: 4LZW).

tions (B) in the E subunit of *Vch*UPh complexed with thymidine and the corresponding residues of the F subunit in the structure of *Vch*UPh complexed with thymidine is 0.17 Å, whereas the rms deviation for another possible position (A) is 0.43 Å.

The double position is attributed to the fact that the binding of the THM molecule causes the displacement of the region involving residues 92 and 93 of the β5 strand toward the ligand (Figs. 3, 6, 7). In the binding sites containing THM with partial occupancy (C and E subunits), one of the alternative positions of the chain region 92–93 corresponds to the ligated state, and the other position corresponds to the unligated one (Fig. 7).

When bound to the residues of the A, B, E, and F subunits of the *Vch*UPh molecule (ID PDB: 4OEH), uracil **(**URA**)** occupies only the uracil-binding subsite of the nucleoside-binding site with full occupancy (Fig. 8).

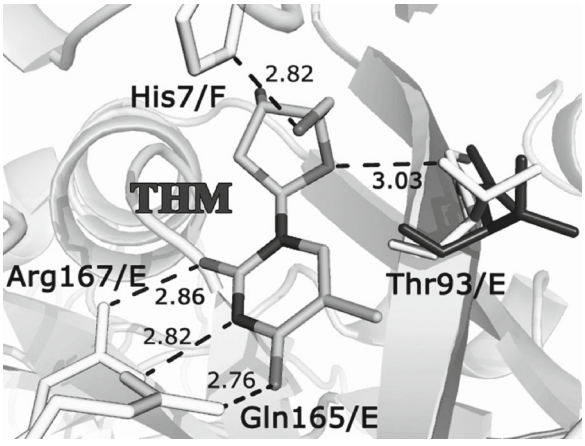

Fig. 7. Alternative conformations of Thr93 in the structure of *Vch*UPh in complex with thymidine.

In the structure of *Vch*UPh complexed with uracil (ID PDB: 4OEH), the URA molecule binds to the nucleoside-binding site through the following hydrogen bonds: OE1_Gln165/F—2.91 Å—N3_URA; NE2_Gln165/F—2.98 Å—O2_URA; NH2_Arg167/F—2.99 Å—O4_URA; O4_URA— 2.83 Å—H2O—2.74 Å—NH2_Arg222/F; O4_URA— 2.33 Å—H2O—2.80 Å—NH2_Arg167/F. The phenyl group of Phe161/F is arranged perpendicular to the aromatic heterocycle of URA and interacts with the latter via herringbone-type π stacking. The nucleoside-binding sites of the subunits of the CD homodimer are unligated.

In the nucleoside-binding site of *Vch*UPh in complex with thymine (ID PDB: 4OGL), the thymine **(**TDR**)** molecule, like URA, is hydrogen-bonded only to the pyrimidine-binding-site residues Gln165, Arg167, and Arg222 (Fig. 9). The TDR molecule was found in all six active sites of the structure of *Vch*UPh complexed with TDR (ID PDB: 4OGL).

In the active sites of the B and E subunits of *Vch*UPh in complex with thymine (ID PDB: 4OGL), the occupancy factor for TDR is 0.73. In these subunits (B and E), residues 92 to 96 are disordered over two conformations. The largest displacement of atoms was observed for the alternative conformations of Thr93/B (for the Cα atom, 1.57 Å; for the Cβ atom, 2.32 Å). The rms deviation between the atomic coordinates of the residues 92–96 in one of the double positions (position A) in the B subunit of *Vch*UPh complexed with thymine and the analogous residues in the A subunit of unligated *Vch*UPh (ID PDB: 3O6V, 1.70 Å resolution, DPI 0.09 Å) is 0.25 Å; for another position

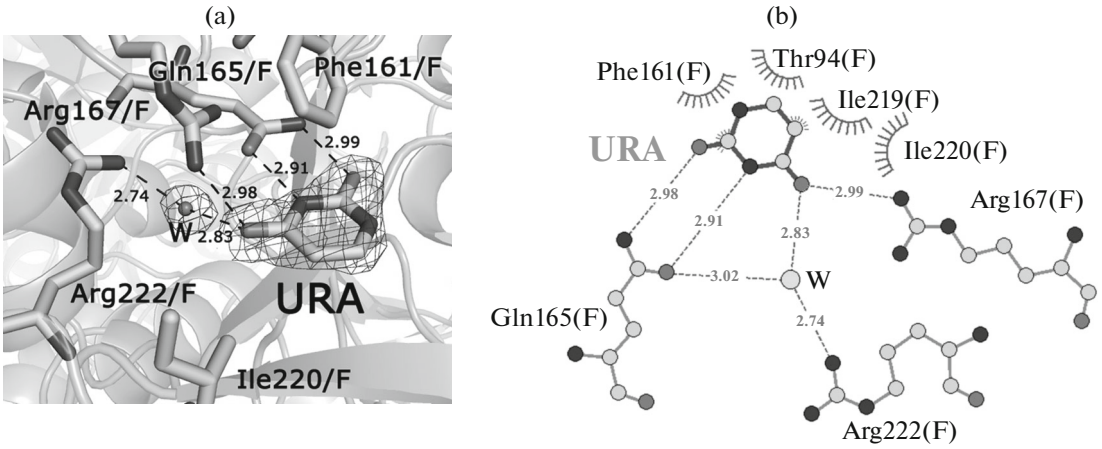

Fig. 8. (a) Active site of *Vch*UPh in complex with uracil (URA, ID PDB: 4OEH). The 2mFo-DFc electron density map is contoured at the 1.5 σ level. (b) The schematic diagram of enzyme–substrate interactions in the structure of *Vch*UPh complexed with uracil (URA, ID PDB: 4OEH).

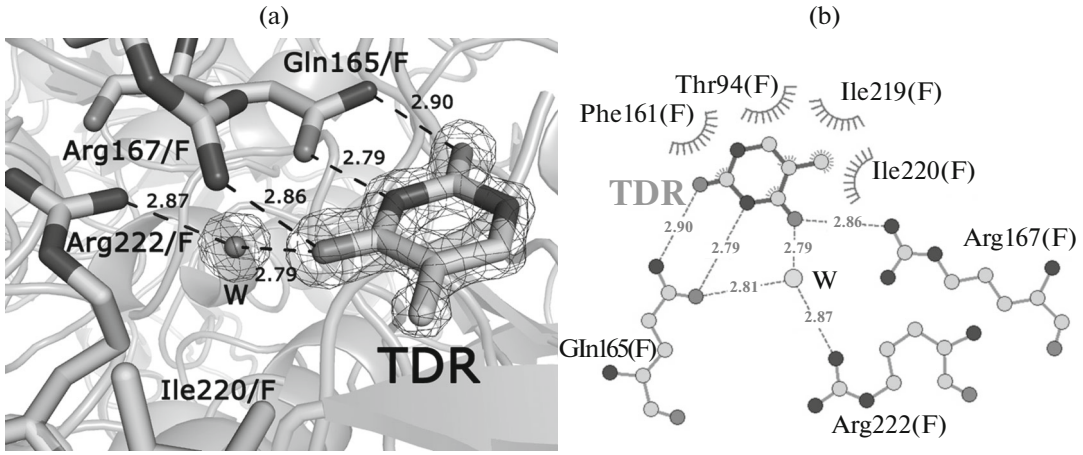

Fig. 9. (a) Active site of *Vch*UPh in complex with thymine (TDR, ID PDB: 4OGL). The 2mFo-DFc electron density map is contoured at the 1.5 σ level. (b) The schematic diagram of enzyme–substrate interactions in the structure of *Vch*UPh complexed with thymine (TDR, ID PDB: 4OGL).

(position B), the rms deviation is 1.32 Å. The rms deviation between the atomic coordinates of the residues 92–96, which adopt two conformations in the B subunit of *Vch*UPh complexed with thymine, and the same residues of the F subunit in the structure of *Vch*UPh complexed with thymine is 0.14 Å for one of the double positions (B) and 1.41 Å for another position (A). Like in the structure of *Vch*UPh complexed with thymidine, one of the alternative positions (B) of these structure elements in the *Vch*UPh + TDR complex corresponds to the ligated state, whereas another position (A) corresponds to the unligated state of the enzyme.

An alternative conformation of the region (residues 92–96) of the β5 strand is attributed not only to the binding of thymine with partial occupancy to the enzyme molecule, but also to the binding of glycerol or Tris to the ribose-binding-site residues. Thus, the Tris molecule forms hydrogen bonds with the key residues of the ribose-binding site, including Thr93 (OG1_Thr93/B—2.72 Å—O1_TRS; NE2_His7/A—3.09 Å—O2_TRS; N_Met196/B—3.13 Å—O3_TRS; OE1_Glu197/B—2.68 Å—O3_TRS: OE2_Glu197/B—2.80 Å—N_TRS). A similar situation is observed in the active site of the E subunit, the residues of which are bound to a glycerol molecule. Therefore, due to the presence of hydroxy groups, glycerol, as well as Tris, mimics the binding of the furanose moiety of ribonucleosides (uridine or thymidine), resulting in changes in the configuration of the β5 strand.

Gate Loop in the Structures of VchUPh Complexes

The loop (L11 in *Vch*UPh) (Fig. 3) in bacterial UPhs was shown to act as a gatekeeper, which controls the access of nucleoside substrates to the active site of the enzyme [5, 48, 50]. In these publications, the authors concluded that the position of the loop may correspond to three functional states of the active

site—open, closed, and intermediate. In the subunits with the open active site, the loop is exposed to the solvent and does not prevent the access of substrate molecules to the active site. In the case of a closed active site, the changes in the conformation of the loop and its subsequent interaction with the protein surface residues (Tyr168 and Asp169) lead to the blockage of the access of substrate molecules to the active site. The concerted movement of the gate loop together with the β5 strand (residues 87–96, according to the numbering used for *Vch*UPh) and the parallel β8 strand (residues 211–221) was described in [5].

Loop L11 in the VchUPh Molecule in Unligated State

The position of the loop L11 always corresponds to the open state of the active site if the binding sites of the enzyme lack ligand molecules (unligated *Vch*UPh; ID PDB: 3O6V). This is observed in the unligated C and D subunits of *Vch*UPh in complex with uracil (ID PDB: 4OEH) and the unligated A and D subunits of *Vch*UPh in complex with phosphate (ID PDB: 4IP0). The residue Ile220 involved in the β8-strand hinders the closure of the active site by the loop L11 in the apo form of *Vch*UPh due to the van der Waals interaction between this residue and the Cα atom of Pro228 of the loop L11; the distance between the interacting atoms is shorter than 3 Å. It should be noted that Val221 in uridine phosphorylases from *Escherichia coli* (ID PDB: 1RXS and 1RXU), *Salmonella typhimurium* (ID PDB: 3FWP), *Homo sapiens* (hUPP1, hUPP2) (ID PDB: 2XRF, 3EUE), and *Shewanella oneidensis* MR-1 (ID PDB: 4R2W), which corresponds to Ile220 in *Vch*UPh, does not interfere with changes in the conformation of the loop and the closure of the active site in the unligated state due to the smaller volume of the side chain (three versus four alkyl carbon atoms).

Conformation of the Loop L11 of VchUPh in the Presence of Pyrimidine Substrates of the Forward/Reverse Reactions in the Active Site of the Enzyme

The conformation of the gate loop L11 corresponds to the closed active site in the B and F subunits of *Vch*UPh complexed with uridine (ID PDB: 5C80), the A and F subunits of *Vch*UPh complexed with thymidine (ID PDB: 4LZW), the B and E subunits of *Vch*UPh complexed with uracil (ID PDB: 4OEH), and the A and F subunits of *Vch*UPh complexed with thymine (ID PDB: 4OGL). For example, in the structure of *Vch*UPh complexed with uracil (ID PDB: 4OEH), the loop L11 in the B subunit forms contacts with the surface of the same subunit through the following hydrogen bonds: NE_Arg167/B—2.93 Å—O_Glu226/B; NH2_Arg167/B—2.73 Å—O _Glu227/B; N_Tyr168/B—2.79 Å—OE2_Glu226/B, and N_Asp169/B—2.95 Å—OE1_Glu226/B. In other cases, in which the loop L11 closes the active site, the hydrogen bonds between the residues are similar to those considered above.

The B factors for the atoms of the loop that closes the active site are 1.5 times higher than the average B factor of the structure. Thus, the average B factor of the main-chain atoms of this loop in the B subunit of *Vch*UPh complexed with uracil is 23.90 Å^2, whereas the average B factor of all main-chain atoms of the structure is 17.18 Å^2. In the case of the open conformation of the active site, the B factors for the atoms of the loop L11 are 2–4 times higher than the average B factor of the structure in all the complexes under consideration. In the structure of *Vch*UPh complexed with uracil, the average B factor for the main-chain atoms of the loop L11 in the C subunit with the open active site is 37.72 Å^2. The maximum values of the B factor are observed for atoms of the residues 228–231 (the average B-factor for the main-chain atoms of this region is 49.52 Å^2). The changes in the B factors for the atoms of the loop L11 upon conformational changes are consistent with those described in [5, 48, 50].

Meanwhile, the conformation of the loop in the B subunit in the structure of *Vch*UPh complexed with thymidine (ID PDB: 4LZW); the A and F subunits in the structure of *Vch*UPh complexed with uracil (ID PDB: 4OEH); and the A, C, D, and E subunits in the structure of *Vch*UPh complexed with uridine (ID PDB: 5C80) corresponds to the open active site, despite the binding of the enzyme to the pyrimidine ligands (Fig. 10).

Therefore, the presence of the pyrimidine substrate (URA, TDR) or the nucleoside substrate (URI, THM) at the nucleoside-binding site is a necessary but insufficient condition for the closed state of the active site and the appropriate conformation of loop L11 when the phosphate-binding site is not occupied by the second substrate.

State of the Active Site and the Conformation of Loop L11 upon Binding of the Phosphate Anion

In the subunits containing the phosphate anion bound to the active-site residues (B, C, and F subunits of *Vch*UPh complexed with phosphate (ID PDB: 4IP0)) (Fig. 4a), only the closed active site and the appropriate conformation of the loop L11 are observed. The conformations of the residues Arg90 and Thr93 (and, consequently, of the region of the β5 strand) differ from those observed in the unligated enzyme (Figs. 2, 4), and these residues are displaced toward the ligand (rmsd are described in the Phosphate-Binding Site section). The conformational changes in the β5 strand lead to the shift of the parallel region of the β8 strand comprising the residues 216–221 toward the binding site; rmsd between the coordinates of the Cα atoms of the residues Ala216, Gly217, Val218, Ile219, Ile220, and Asn221 of *Vch*UPh ligated by the phosphate anion and the corresponding atoms

of the enzyme in the free state are 0.6, 0.9, 0.7, 1.0, 0.8, and 0.5 Å, respectively. These changes are accompanied by the displacement of the region comprising the residues 101–106 (a fragment of the loop L5) and the β6-strand; rmsd between the coordinates of the Cα atoms of the residues Val101, Asn102, Val103, Gly104, Asp105, and Met106 of *Vch*UPh ligated by the phosphate anion and the corresponding atoms of the enzyme in the free state are 0.5, 0.5, 0.6, 1.0, 0.8, and 0.6 Å, respectively (Figs. 2, 3). In turn, the displacement of the β8 strand causes a change in the conformation of the first residues of loop L11 (Arg222, Thr223), thus fastening the loop in the position characteristic of the closed state of the active site.

The transformation of the β5 strand and loop L11 to the state corresponding to the closed active site and the fixation in this state by the phosphate anion occur through the simultaneous binding of the phosphate anion to Arg90 and Thr93 of the β5 strand and to Gly25 of the β1 strand (Phosphate-Binding Site section; Figs. 3, 4). As opposed to the phosphate anion, the ribose moiety of nucleosides binds only to Thr93 of the β5 strand. Therefore, the position of the β5 strand with respect to the β1 strand varies and the loop L11 can adopt a conformation characteristic not only of the closed active site, but also of other states of the active site (Figs. 2, 4a, 4b).

In the case of the UPh-catalyzed forward reaction, the phosphate anion acts as the second substrate bound at the active site. Upon the binding of phosphate at the active site, loop L11 is fixed in the conformation that closes the active site, thus preventing the access of nucleosides to the binding site. In addition, the binding of the phosphate anion leads to the narrowing of the active-site region between the β5 and β1 strands, which promotes the enzymatic reaction (Figs. 2, 3, 4b). The scheme of successive conformational changes in the enzyme induced by the binding of the substrates of the forward reaction is presented in Fig. 11.

Influence of the Crystal Packing on the Conformation of Loop L11

In the case of the intermediate state of the active site, the conformation of loop L11 in the C subunit of *Vch*UPh complexed with thymidine (ID PDB: 4LZW) is such that the loop is not exposed to the solvent and it forms the following hydrogen bonds with residues of the adjacent hexameric molecule: NE2_Gln224/C—3.08 Å—O_Gly173/F*, OD1_Asp229/C—3.26 Å—O_Arg222/F*, N_His230/C—2.85 Å—O_Thr223/F*, N_Ala231/C—2.84 Å—O_Gln224/F* (residues of the adjacent molecule are marked with an asterisk) (Fig. 12). Loop L11 in the C subunit of *Vch*UPh complexed with thymidine does not form hydrogen bonds characteristic of the closed state of the active site, such as the hydrogen bond of Glu226/C with Asp169/C and the hydrogen bonds of Tyr168/C and Glu227/C with Asp169/C, but it forms hydrogen bonds with other residues of the same subunit: NE_Arg167/C—2.77 Å—OE1_Glu226/C; NE_Arg167/C—3.03 Å—NH2_Glu226/C. The conformation of loop L11 in the F* subunit is characteristic of the closed active site.

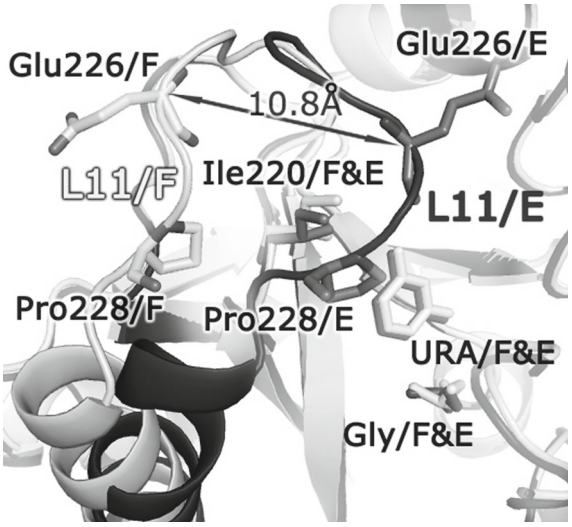

Fig. 10. Superposition of the three-dimensional structures of the F and E subunits of *Vch*UPh in complex with uracil (ID PDB: 4OEH). The positions of the loops correspond to the open (L11/F) and closed (L11/E) active sites. The distance between the Cα atoms of Glu226 of the loop L11, which adopts different conformations in the subunits with the open and closed active site, is indicated by an arrow.

The position of the loop is most influenced by the abovementioned hydrogen bonds between the main-chain atoms of adjacent molecules (C and F* subunits). The presence of these hydrogen bonds leads to conformational changes of the residues 228–231 of loop L11 in the C subunit. A comparison of the loops in the subunits, in which the active site is in the intermediate and closed states, shows that rmsd between the coordinates of the Cα atoms of the residues Pro228, Asp229, His230, and Ala231 are 3.8, 4.1, 4.0, and 4.2 Å, respectively. The interactions of residues Ala231/C and His230/C of loop L11 with residues Arg222/F* and Gln224/F* of the adjacent molecule interfere with the formation of hydrogen bonds of Glu226/C with Tyr168/C and Asp169/C characteristic of the closed active site and the appropriate conformation of the loop L11. Therefore, loop L11 in the C subunit adopts a conformation observed for the intermediate state of the active site.

A similar conformation of loop L11 was observed in the D subunit of *Vch*UPh complexed with thymidine (ID PDB: 4OGL), the C and D subunits of *Vch*UPh complexed with thymine (ID PDB: 4OGL), and for uridine phosphorylases from *Salmonella typhimurium* (ID PDB: 3FWP) and *Shewanella oneidensis* MR-1 (ID PDB: 4R2W).

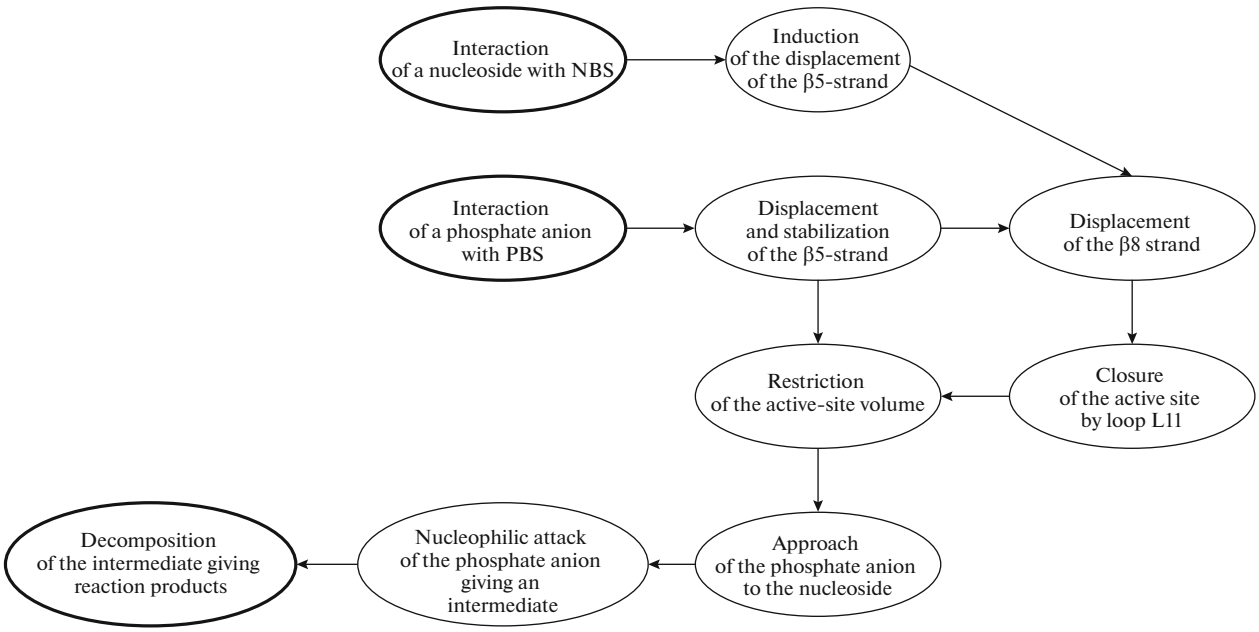

Fig. 11. Scheme of successive conformational changes in the enzyme induced by the binding of substrates of the forward reaction.

The molecular dynamics simulation revealed a set of intermediate states of the loop L11 in an individual *Vch*UPh molecule in solution. However, the lifetime of these states is much shorter that the time during which the conformation of the loop corresponds to the closed or open active site of the subunit. Probably the conformation of loop L11 characteristic of the intermediate state of the active site that is observed in the *Vch*UPh complex is a consequence of interactions between adjacent enzyme molecules in the crystalline state.

Mechanisms of Nucleoside Recognition by VchUPh and the β-N1-Glycosidic Bond Cleavage in Substrates of the Forward Reaction

The side group of the residue Gln165 in *Vch*UPh, which is conserved in bacterial UPhs (Figs. 3, 5, 6) (ID PDB: 4LZW, 5C80, 4OEH, 4OGL) and which corresponds to Gln166 in *St*UPh and *Ec*UPh [5, 22, 48], plays a key role in the recognition and binding of the heterocyclic moiety of the substrate. In all the abovementioned structures, this residue is oriented so that its positively charged amide group forms a hydrogen bond with the negatively charged O2 atom of the substrates of both the forward (pyrimidine nucleosides—uridine and thymidine) and reverse (pyrimidine bases—uracil and thymine) reactions. Thus, there are the following hydrogen bonds in *Vch*UPh:

NE2_Gln165/F/*Vch*UPh—2.87 Å—O2_THM;
NE2_Gln165/F/*Vch*UPh—2.90 Å—O2_TDR;
NE2_Gln165/F/*Vch*UPh—2.98 Å—O2_URA;
NE2_Gln165/F/*Vch*UPh—2.66 Å—O2_URI

(Figs. 5, 6). In turn, the negatively charged carbonyl group of Gln165 in *Vch*UPh forms a hydrogen bond with the positively charged N3 atom of the pyrimidine heterocycle of the ligand: OE1_Gln165/F/*Vch*UPh—2.80 Å—N3_THM; OE1_Gln165/F/*Vch*UPh—2.79 Å—N3_TDR; OE1_Gln165/F/*Vch*UPh—2.91 Å—N3_URA; OE1_Gln165/F/*Vch*UPh—2.72 Å—N3_URI (Figs. 5, 6). Similar hydrogen bonds are present in the structures of the complexes of *St*UPh and *Ec*UPh with ligands [5, 22, 48].

The functional groups containing O2 and N3 atoms are present both in the uridine and thymidine molecules, which facilitates the recognition and binding of these two ligands by UPh. According to the results of chemical kinetics, the affinity of bacterial UPhs of the NP-1 family for uridine is 2.5 times higher than the affinity for thymidine [1, 2, 20].

Let us consider the main structural–functional aspects of the β-N1-glycosidic bond cleavage in the substrate of UPhs of the NP-1 family. First, electrostatic interactions of the active-site residues induce the electron redistribution in the nucleoside molecule with a decrease in the electric-charge difference between the N1 and C1′ atoms of the ligands [5, 20, 51]. This process leads to a weakening of the β-N1-glycosidic bond. Second, the ribose moiety of both uridine and thymidine (ID PDB: 5C80, 4LZW), which are substrates of the forward reaction catalyzed by *Vch*UPh and *Ec*UPh [5, 20, 51], binds to the active-site residues (Thr93, Met196, Asp197 in *Vch*UPh) in the strained high-energy conformation (Figs. 5, 6). It was found that the conformation of the uridine molecule at the active sites of *Vch*UPh (ID PDB: 5C80) and *Ec*UPh [5, 20, 51] differs from that observed in solution [52]. Thus, the pyrimidine ring of the ligand is in the *sin* position with respect to the furanose moiety,

and the C1'–C2'–C3'–C4'–O4' fragment of the furanose ring of the substrate has a planar structure.

The binding of substrates in high-energy conformations results in an overlap of the electron orbitals between the Cl'–Nl and C2'–H2' bonds in the ligand molecules, resulting in a weakening of the β-N1-glycosidic bond. These processes lead to a decrease in the potential energy barrier for the β-N1-glycosidic bond cleavage, and the nucleophilic attack on this bond by the phosphate anion induces the enzymatic reaction [5, 20, 51]. Taking into account the high structural homology between the active sites of bacterial UPhs, it can be hypothesized that this reaction mechanism is common to all enzymes of this group, including *Vch*UPh.

Structural Aspect of the Influence of the 2-Hydroxy Group of the Ribose Moiety of Nucleosides on the Enzymatic Reaction Rate

The rms deviation between the coordinates of the Cα atoms of the active-site residues in the structures of *Vch*UPh complexed with uridine (ID PDB: 5C80; the FE homodimer) and *Vch*UPh complexed with thymidine (ID PDB: 4LZW; the FE homodimer) is 0.178 Å; between the coordinates of all atoms of the active-site residues, 0.257 Å; and between the side chains of the residues, 0.290 Å. Therefore, the binding sites in *Vch*UPh complexed with uridine (ID PDB: 5C80) and *Vch*UPh complexed with thymidine (ID PDB: 4LZW) are structurally identical.

The rms deviation between the atomic coordinates of the uridine and thymidine molecules in *Vch*UPh complexed with uridine (ID PDB: 5C80) and thymidine (ID PDB: 4LZW) is 0.603 Å (Fig. 13). The rms deviation between the atomic coordinates of the pyrimidine moieties of uridine and thymidine is 0.396 Å. The parallel displacement in the plane of the pyrimidine rings of uridine and thymidine with respect to one another is not observed (Fig. 13).

The calculated energy of the conformation for the main state of uridine in solution is $E'_{water} = 100.1$ kJ/mol; for uridine bound at the active site of *Vch*UPh in the crystalline state, $E'_{UPh} = 186.9$ kJ/mol (ID PDB: 5C80). For thymidine $E'_{water} = 107.2$ and $E'_{UPh} = 165.3$ kJ/mol (ID PDB: 4LZW). The energy difference between the conformations of the ligands bound at the active site of the *Vch*UPh complexes in the crystalline state and in aqueous solution is 86.8 and 58.1 kJ/mol for uridine and thymidine, respectively. Therefore, the formation of two additional hydrogen bonds (N_Met196/A—3.14 Å—O2'_URI; OE1_Glu197/A—2.56 Å—O2'_URI) with the 2'-hydroxy group of uridine (Fig. 5) not only leads to an increase in the binding energy, as was noted earlier for the *Ec*UPh + URI complex [5], but also results in the more strained *twist* C1'-endo/O4'-exo (^1T_o) conformation of the uridine molecule as opposed to the C1'-endo (^1E) conformation of the thymidine molecule (Fig. 13).

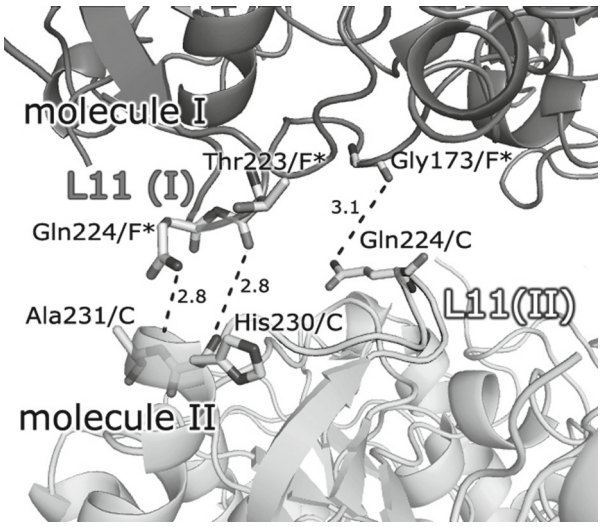

Fig. 12. Amino-acid residues of a fragment of the C subunit (molecule II) in the structure of *Vch*UPh complexed with thymidine, which form hydrogen bonds with the F* subunit of the adjacent hexameric molecule (molecule I). The region of loop L11 of the C subunit is labeled L11 (II); that of the F* subunit labeled L11 (I).

The difference between the energies E'_{water} and E'_{UPh} of the uridine molecule in the active site of *Vch*UPh is 28.7 kJ/mol larger than that for the thymidine molecule, which facilitates the cleavage of the β-N1-glycosidic bond between the pyrimidine and ribose moieties of uridine and leads to an increase in the rate of the reaction with uridine.

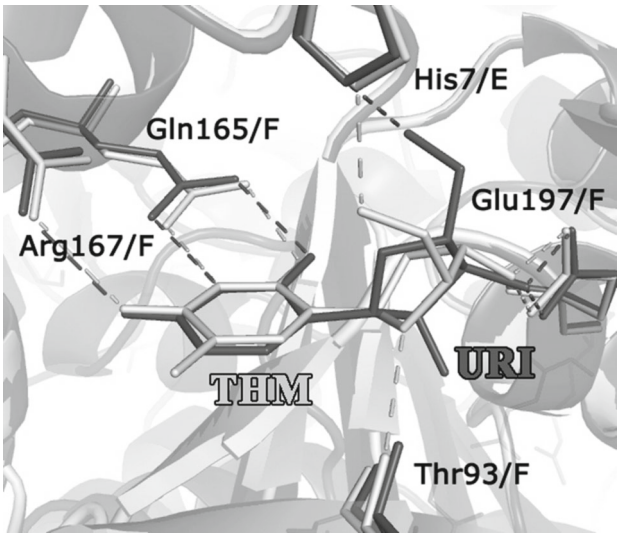

Fig. 13. Superposition of the three-dimensional structures of *Vch*UPh in complexes with uridine (URI, ID PDB: 5C80) and thymidine (THM, ID PDB: 4LZW).

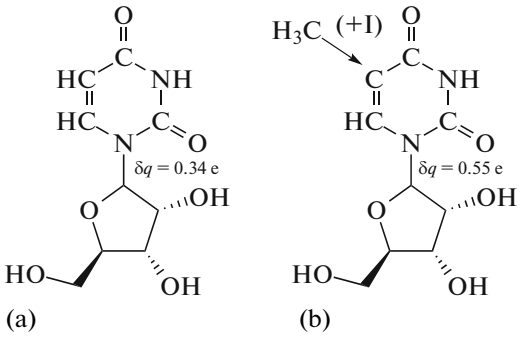

Fig. 14. Difference in the partial electric charges on atoms that form the β-N1-glycosidic bond in (a) uridine and (b) 5-methyluridine.

Therefore, the interactions of the 2'-hydroxy group of uridine with atoms of the active-site residues Met196 and Glu197 of *Vch*UPh play a considerable, if not key, role in the different affinity of UPh for uridine and thymidine. This is consistent with the results reported in [1, 5, 20]. However, these interactions not only lead to an increase in the binding energy of uridine to the active-site residues [1, 5, 20] but are also responsible for the ribose moiety of uridine adopting a higher energy (i.e., more reactive) conformation (C1'-endo/O4'-exo($'T_o$)) compared to thymidine (Figs. 5, 13).

Structural and Quantum-Chemical Aspects of the Influence of the 5-Methyl Group of the Pyrimidine Moiety of Nucleosides on the Enzymatic Reaction Rate

The 5-methyl group of thymidine is located in the vicinity of the residues that form the hydrophobic environment of the ligand: CG2_Ile220/F—3.68 Å—CM5_THM; CD1_Ile219/F—3.60 Å—CM5_THM; CG1_Ile219/F—3.55 Å—CM5_THM (Fig. 6). There is no steric hindrance to the binding of thymidine at the active site because the distances between the methyl carbon atoms of the residues and the methyl group CM5 of thymidine are larger than 3.4 Å. Therefore, the 5-methyl group of thymidine cannot hinder the binding of this substrate at the active site of bacterial UPhs, in particular, of *Vch*UPh (Figs. 6, 13). Despite this fact, the presence of the methyl group at the 5 position of the pyrimidine heterocycle of the ligand leads to a decrease in the enzymatic reaction rate, as was shown for the thymidine analog—5-methyluridine [1, 2, 20]. The 5-methyluridine molecule differs from uridine in that it contains the methyl group at the 5 position of the heterocycle (like in the thymidine molecule), whereas the furanose moiety of these ligands has the same structure. Based on the experimental and calculated data, a decrease in the reaction rate due to the presence of the methyl group at the 5 position of the pyrimidine ring is attributed to its effect on the electronic structure of the substrate. Thus, the partial charge difference between the N1–C1' atoms in 5-methyluridine, which is an analog of thymidine, is $\Delta\delta q = 0.55$ e; in uridine, $\Delta\delta q = 0.34$ e. This is associated with the positive inductive effect (I+) of the 5-methyl group on the aromatic ring (Fig. 14). The larger difference in the magnitudes of the partial charges on the atoms of the β-N1-glycosidic bond in the 5-methyluridine molecule compared to that in uridine leads to the stabilization of this bond in 5-methyluridine (and, by analogy, in the thymidine molecule) and a decrease in the rate of phosphorolytic cleavage of thymidine and 5-methyluridine compared to uridine. This conclusion is consistent with the biochemical results [20], which showed that the affinity of *Ec*UPh for uridine is higher than that for 5-methyluridine, the binding-site residues being completely homologous.

The negative effect of methyl group CM5 on the enzymatic reaction rate may be attributed to the fact that the positive inductive effect of the 5-methyl group attached to the pyrimidine moiety of this ligand causes a change in the partial charge on the N1 atom of thymidine. A change in the charge on the N1 atom of thymidine leads to the additional stabilization of the β-N1-glycosidic bond between the pyrimidine and ribose moieties of thymidine and a decrease in the enzymatic reaction rate compared to that with uridine.

Influence of the 5-Methyl Group of the Pyrimidine Moiety of Nucleosides on the Strain of the Covalent β-N1-Glycosidic Bond

A comparison of the structures of *Vch*UPh complexed with uridine (ID PDB: 5C80; the F subunit) and *Vch*UPh complexed with uracil (ID PDB: 4OEH; the B subunit), which is the product of the forward phosphorolysis reaction, revealed the difference in the positions of the pyrimidine rings of these ligands (rmsd between the atomic coordinates is 0.470 Å) (Fig. 15a). The rms deviation between the coordinates of all atoms of the active sites in the crystal structures of these complexes is 0.274 Å; between the atomic coordinates of the side chains of the active-site residues it is 0.278 Å. In the structure of *Vch*UPh complexed with uridine, the center of the pyrimidine moiety of uridine moves closer toward the OE2 atom of the residue Glu197 by 0.6 Å compared to the center of the pyrimidine ring of uracil (Fig. 15a).

However, a comparison of the three-dimensional structures of *Vch*UPh complexed with thymine (ID PDB: 4OGL, the F subunit) and of *Vch*UPh complexed with thymidine (ID PDB: 4LZW, the F subunit) did not reveal significant differences in the atomic coordinates of the pyrimidine rings of these ligands (rmsd between the atomic coordinates is 0.215 Å; see Table 4) and in the distances between the centers of the pyrimidine rings and the OE2 atom of residue Glu197 (Fig. 15b). This fact is attributed to the presence of the methyl group in the thymine molecule, which is absent in uracil and which hinders the

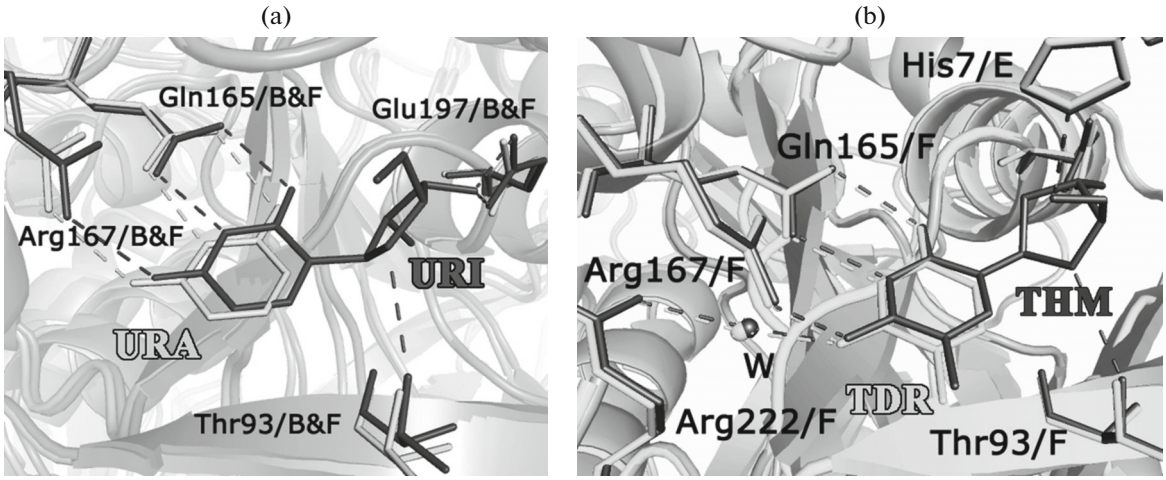

Fig. 15. Superposition of selected active-site residues (a) in the structures of *Vch*UPh in complexes with uridine (URI) and uracil (URA) and (b) in the structures of *Vch*UPh in complexes with thymine (THM) and thymidine (TDR).

interaction between the thymine molecule and Ile220 and, correspondingly, prevents Glu197 from mowing away, as opposed to the uracil molecule.

Therefore, the formation of the covalent β-N1-glycosidic bond between the ribose moiety and the pyrimidine base in the uridine molecule (Figs. 5, 15a) results in the center of the pyrimidine ring moving 0.6 Å closer to the ribose-binding site compared to the center of the pyrimidine ring of the uracil molecule. This gives rise to additional strain of the β-N1-glycosidic bond in the uridine molecule compared to thymidine (Figs. 5, 15a), which leads to the bond cleavage in the course of the chemical reaction, and, as a consequence, in an increase in the rate of the forward phosphorolysis reaction of uridine compared to the phosphorolysis of thymidine.

Structural and Quantum-Chemical Aspects of the Influence of the 5-Methyl Group of Nitrogenous Bases on the Rate of the Reverse Enzymatic Reaction

A comparison of the structures of *Vch*UPh in complexes with uracil (ID PDB: 4OEH) and thymine (ID PDB: 4OGL) demonstrates that the conformations and positions of the binding-site residues and residues involved in the hydrophobic environment of the ligand are identical in both structures (Fig. 16). The rms deviation between the atomic coordinates of the active-site residues of *Vch*UPh in complexes with uracil (AB homodimer, ID PDB: 4OEH) and thymine (EF homodimer, ID PDB: 4OGL) is 0.228 Å; between the atomic coordinates of the side chains of the active-site residues, it is 0.230 Å.

The rms deviation between the atomic coordinates of uracil (ID PDB: 4OEH) and thymine (ID PDB: 4OGL) bound at the active sites is 0.345 Å (Fig. 16). The X-ray diffraction study of the structures of *Vch*UPh complexed with uracil and thymine showed that the distance between the C5 atom of thymine and CG2_Ile220 is 0.4 Å larger (Fig. 16) than that with uracil due to van der Waals interactions between the 5-methyl group of thymine and the side-chain atoms of Ile220. It should be noted that this arrangement of thymine in the active site in the presence of the second substrate results in the distance between the reactive C1' and N1 atoms, which form the β-N1-glycosidic bond between the pyrimidine and ribose moieties of the nucleoside in the course of the nucleoside synthesis, being ~0.4 Å shorter than that in the case of uracil (Fig. 16). This leads to an increase in the rate of the reverse reaction with thymine in the presence of the chemically identical second substrate (for example, aribose 1-phosphate).

The methyl group of thymine, being an orienting agent of the first type, induces a partial positive charge on the N1 atom of the heterocyclic ring of thymine (Fig. 17). This leads to a decrease in the magnitude of the negative electric charge on the N1 atom of the thymine molecule, resulting in a lower nucleophilic activity of thymine compared to uracil.

Influence of the Chemical Structure and the Conformation of the Furanose Moiety of the Second Substrate on the Rate of the Reverse Enzymatic Reaction

In our opinion, the chemical structure and the conformation of the furanose moiety of the second substrate (ribose 1-phosphate or 2-deoxyribose 1-phosphate) have a more considerable effect on the rate of the uridine phosphorylase-catalyzed synthesis of uridine from uracil and of thymidine from thymine. This hypothesis was confirmed by molecular docking of the second substrates of the reverse reaction—ribose 1-phosphate or 2-deoxyribose 1-phosphate—to the active sites of *Vch*UPh complexed with uracil

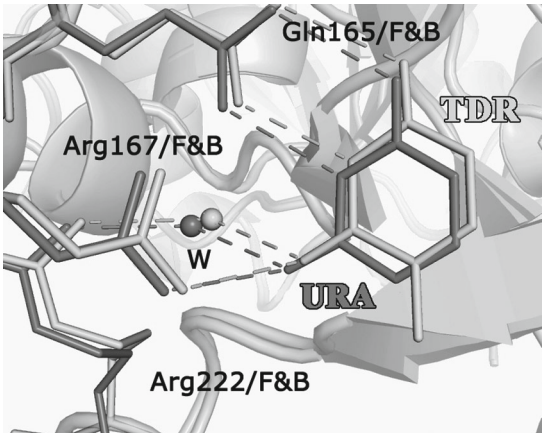

Fig. 16. Superposition of selected binding-site residues in the structures of *Vch*UPh in complexes with thymine (TDR) and uracil (URA).

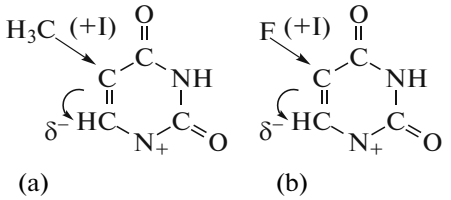

Fig. 17. Electronic effects of the substituents at the 5 position of the nitrogenous bases (a) thymine and 5-fluorouracil (b).

(Fig. 18a) and thymine (Fig. 18b). The molecular docking was performed without the exclusion of the atomic coordinates of thymine and uracil from the corresponding structures of the complexes.

The calculations performed for ribose 1-phosphate and 2-deoxyribose 1-phosphate gave solutions which do not differ in the position of the phosphate group but differ in the conformation of the furanose ring—C1'-endo/O4'-exo (^1T_o) for the former ligand and C1'-endo (^1E) for the latter one. The energy difference between the conformations in solution and in the complex with the enzyme in the crystalline state is 69.2 kJ/mol for ribose 1-phosphate and 37.8 kJ/mol for 2-deoxyribose 1-phosphate. The energy difference is attributed to the formation of a hydrogen-bond network between the 2-hydroxy group of ribose 1-phosphate (R1P) and the ribose-binding-site residues of *Vch*UPh: N_Met196/F—3.11 Å—O2'_R1P; OE1_Glu197/F—2.80 Å—O2'_R1P; NH2_Arg90—3.10 Å—O2'_R1P (Fig. 18a). The 2-deoxyribose 1-phosphate molecule does not form similar bonds with the residues of the enzyme due to the lack of the 2-hydroxy group in the ligand (Fig. 18b). It should be noted that the calculated energy difference between the conformations of ribose 1-phosphate in solution and this ligand bound to *Ec*UPh in complex with uracil and ribose 1-phosphate (ID PDB: 1TGY) is 75.2 kJ/mol. This is consistent with the estimation of the energy of *Vch*UPh in complex with ribose 1-phosphate and uracil, which was studied by molecular docking. The higher energy conformation of the second substrate (ribose 1-phosphate) leads to an increase in the rate of the chemical reaction compared to 2-deoxyribose 1-phosphate.

Structural and Quantum-Chemical Aspects of the Influence of the Fluorine Atom of 5-Fluorouracil on the Rate of the Reverse Enzymatic Reaction

It is interesting to analyze the position of the uracil derivative, 5-fluorouracil (5FU), which is also a substrate of the UPh-catalyzed reverse reaction [53–55], at the binding site of bacterial UPh and compare it with the positions of thymine and uracil.

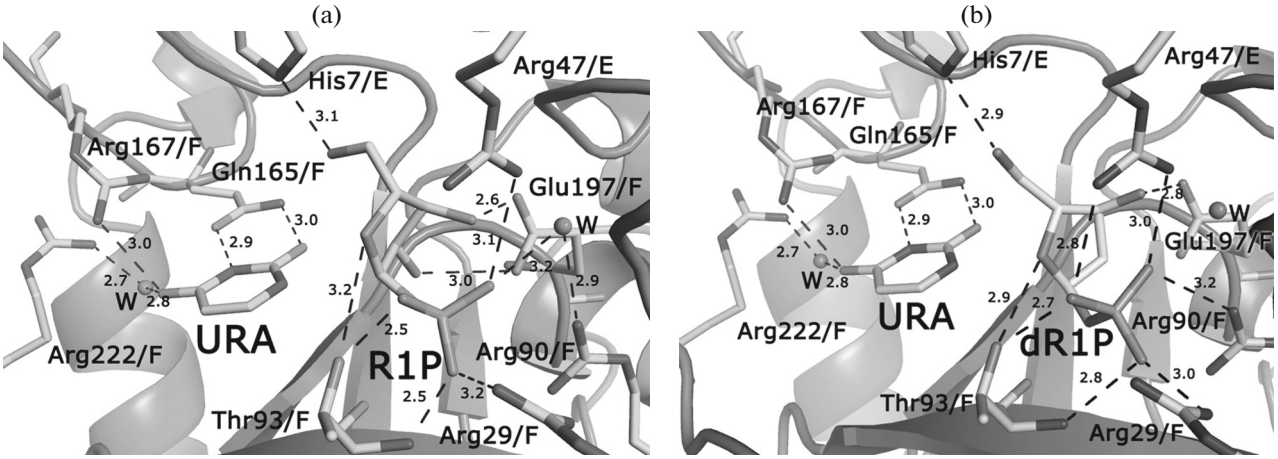

Fig. 18. Three-dimensional structures of the binding sites of *Vch*UPh in (a) complex with ribose 1-phosphate (R1P) and uracil (URA) and (b) in complex with uracil (URA) and deoxyribose 1-phosphate (dR1P).

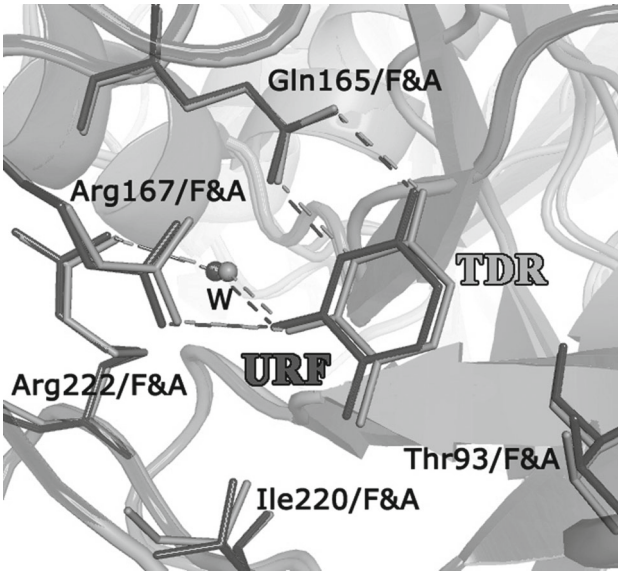

Fig. 19. Superposition of selected active-site residues of *Vch*UPh in complexes with thymine (TDR) and of *St*UPh in complex with 5-fluorouracil (URF) (ID PDB: 4E1V).

A comparison of the binding sites of *Vch*UPh complexed with uracil (ID PDB: 4OEH) and of *St*UPh complexed with 5-fluorouracil (URF) (ID PDB: 4E1V [47]) showed that the conformations of the ligand-binding-site residues are identical (rmsd between the atomic coordinates of the binding-site residues is 0.315 Å). As opposed to the position of thymine in *Vch*UPh, the position of 5-fluorouracil in the structure of *St*UPh [47] is identical to the position of uracil at the binding site of *Vch*UPh (ID PDB: 4OEH) (rmsd between the atomic coordinates of the aromatic ring of the ligands is 0.198 Å). This may be attributed to the fact that the van der Waals radius of fluorine (~1.1 Å) in the 5-fluorouracil molecule is smaller than the van der Waals radius of the methyl group (~2.0 Å) of thymine. The fluorine atom in the complex with 5-fluorouracil is practically not involved in interactions with the hydrophobic environment of the binding site of UPh (Ile220, Ile219) as opposed to the methyl group of thymine (Fig. 19).

The fluorine atom, like the methyl group of thymine, is an orienting agent of the first type and it also causes a decrease in the negative electric charge on the N1 atom of the ligand. Therefore, the presence of the fluorine atom at the 5 position of the aromatic ring of the ligand leads to a decrease in the rate of the reverse reaction with 5-fluorouracil compared to that with uracil. It should be noted that the fluorine atom is the most electronegative substituent (3.98 on Pauling's electronegativity scale versus 2.55 for the sp^3-hybridized carbon atom of the methyl group of thymine) and more strongly withdraws electron density from the aromatic heterocycle of 5-fluorouracil, thus decreasing (compared to thymine) the rate of the UPh-catalyzed reverse reaction with 5-fluorouracil.

CONCLUSIONS

The three-dimensional structures of uridine phosphorylase from the pathogenic bacterium *Vibrio cholerae* in complexes with the substrates of the forward and reverse reactions, such as phosphate anion, uridine, thymidine, uracil, and thymine, were determined with high accuracy by X-ray crystallography (ID PDB: 5C80, 4IP0, 4LZW, 4OEH, 4OGL) and then analyzed.

It was shown for the first time that the formation of a hydrogen-bond network between the 2'-hydroxy group of uridine and the active-site residues of uridine phosphorylases, in particular, of *Vch*UPh (N_Met196/A—3.14 Å—O2'_URI; OE1_Glu197/A—2.56 Å—O2'_URI), results in the ribose moiety of uridine having a higher energy (and, consequently, more reactive) conformation compared to thymidine (71.9 kJ/mol versus 58.1 kJ/mol).

It was revealed for the first time that the positive inductive effect of the 5-methyl group of thymidine on the aromatic ring of this substrate leads to the stabilization of the β-N1-glycosidic bond of nucleoside and a decrease in the rate of the enzyme-catalyzed phosphorolysis of thymidine compared to that of uridine. In addition, the smaller local strain of the β-N1-glycosidic bond in the thymidine molecule bound to the residues of uridine phosphorylase than that in uridine leads to a higher stability of the β-N1-glycosidic bond and lower reactivity of thymidine compared to uridine.

It was shown for the first time that the specificity of uridine phosphorylases toward phosphorylated monosaccharides (2-deoxyribose 1-phosphate and ribose 1-phosphate), as well as toward the ribose moieties of uridine and thymidine, is attributed to interactions of the active-site residues with the 2-hydroxy group of the ligand and, correspondingly, to the energy difference between the conformations of phosphorylated monosaccharides. For the ribose 1-phosphate molecule, $\Delta E' = 69.2$ kJ/mol; for the 2-deoxyribose 1-phosphate molecule, $\Delta E' = 37.8$ kJ/mol.

It was shown that the phosphate anion, which is the second substrate bound at the active site, interacts with the residues Arg90 and Thr93 of the β5-strand and the residue Gln25 of the β1-strand through hydrogen bonds and secures the functional loop L11 in the conformation, in which the active site of the enzyme molecule is not accessible for the binding of nucleosides—uridine or thymidine. The presence of a substrate molecule in the nucleoside-binding site is a necessary but insufficient condition for the closed state of the active site and the appropriate conformation of loop L11 and, consequently, for the preparation of the enzyme to the catalytic event because these ligands, as opposed to the phosphate anion, are bound only to Gln25 of the β5 strand (Figs. 2, 3, 4b).

ACKNOWLEDGMENTS

This study was performed using the budgetary funding for the Shubnikov Institute of Crystallography of Federal Scientific Research Centre "Crystallography and Photonics" of the Russian Academy of Sciences and was supported by the Russian Foundation for Basic Research, project no. 14-04-00952-a.

REFERENCES

1. A. Vita, A. Amici, T. Cacciamani, et al., Int. J. Biochem. **18** (5), 431 (1986).
2. J. C. Leer, K. Hammer-Jespersen, and M. Schwartz, Eur. J. Biochem. **75** (1), 217 (1977).
3. M. V. Dontsova, Y. A. Savochkina, A. G. Gabdoulkhakov, et al., Acta Crystallogr. D **60** (4), 709 (2004).
4. N. S. Brown and R. Bicknell, Biochem J. **334** (1), 1 (1998).
5. T. T. Caradoc-Davies, S. M. Cutfield, I. L. Lamont, et al., J. Mol. Biol. **337** (2), 337 (2004).
6. K. Katsumata, H. Tomioka, T. Sumi, et al., Cancer Chemother. Pharmacol. **51** (2), 155 (2003).
7. P. J. Finan, P. A. Koklitis, E. M. Chisholm, et al., Br. J. Cancer **50** (5), 711 (1984).
8. A. Leyva, I. Kraal, J. Lankelma, et al., Anticancer Res. **3** (4), 227 (1983).
9. A. Kanzaki, Y. Takebayashi, H. Bando, et al., Int. J. Cancer **97** (5), 631 (2002).
10. C. Luccioni, J. Beaumatin, V. Bardot, et al., Int. J. Cancer **58** (4), 517 (1994).
11. T. Ishikawa, M. Utoh, N. Sawada, et al., Biochem. Pharmacol. **55** (7), 1091 (1998).
12. B. Reigner, K. Blesch, and E. Weidekamm, Clin. Pharmacokinet. **40** (2), 85 (2001).
13. J. Schuller, J. Cassidy, E. Dumont, et al., Cancer. Chemother. Pharmacol. **45** (4), 291 (2000).
14. M. Venturini, Eur. J. Cancer **38** (Suppl. 2), 3 (2002).
15. E. Sivridis, Adv. Exp. Med. Biol. **476**, 297 (2000).
16. T. P. Roosild, S. Castronovo, M. Fabbiani, et al., BMC Struct. Biol. **9**, 14 (2009).
17. M. H. el Kouni, F. N. Naguib, J. G. Niedzwicki, et al., J. Biol. Chem. **263** (13), 6081 (1988).
18. B. M. Jimenez, P. Kranz, C. S. Lee, et al., Biochem. Pharmacol. **38** (21), 3785 (1989).
19. C. S. Lee, B. M. Jimenez, and W. J. O'Sullivan, Mol. Biochem. Parasitol. **30** (3), 271 (1988).
20. K. S. Alekseev, Candidate's Dissertation in Chemistry (Engelhardt Institute of Molecular Biology, Moscow, 2012).
21. A. A. Lashkov, A. G. Gabdulkhakov, I. I. Prokofev, et al., Acta Crystallogr. F **68** (11), 1394 (2012).
22. I. I. Prokofev, A. A. Lashkov, A. G. Gabdulkhakov, et al., Acta Crystallogr. F **70**, Part 1, 60 (2014).
23. M. Zolotukhina, I. Ovcharova, S. Eremina, et al., Res. Microbiol. **154** (7), 510 (2003).
24. W. Kabsch, Acta Crystallogr. D **66** (2), 133 (2010).
25. P. Evans, Acta Crystallogr. D **62**, Part 1, 72 (2006).
26. A. Vagin and A. Teplyakov, J. Appl. Crystallogr. **30** (6), 1022 (1997).
27. A. J. McCoy, R. W. Grosse-Kunstleve, P. D. Adams, et al., J. Appl. Crystallogr. **40**, Part 4, 658 (2007).
28. P. D. Adams, P. V. Afonine, G. Bunkoczi, et al., Acta Crystallogr. D **66**, Part 2, 213 (2010).
29. G. N. Murshudov, A. A. Vagin, and E. J. Dodson, Acta Crystallogr. D **53** (3), 240 (1997).
30. P. Emsley and K. Cowtan, Acta Crystallogr. D **60** (12), 2126 (2004).
31. P. Emsley, B. Lohkamp, W. G. Scott, et al., Acta Crystallogr. D **66** (4), 486 (2010).
32. R. A. Laskowski, M. W. MacArthur, D. S. Moss, et al., J. Appl. Crystallogr. **26** (2), 283 (1993).
33. V. B. Chen, W. B. Headd. J. J. Arendall, et al., Acta Crystallogr. D **66** (1), 12 (2010).
34. W. L. Delano, *The PyMOL Molecular Graphics System* (2002). URL: http://www.pymol.orgciteulike-article-id:2816763.
35. M. A. Larkin, G. Blackshields, N. P. Brown, et al., Bioinformatics **23** (21), 2947 (2007).
36. X. Robert and P. Gouet, Nucl. Acids Res. **42**, 320 (2014).
37. A. C. Wallace, R. A. Laskowski, and J. M. Thornton, Protein Sci. **5** (6), 1001 (1996).
38. A. D. Bochevarov, E. Harder, T. F. Hughes, et al., Int. J. Quantum Chem. **113** (18), 2110 (2013).
39. C. R. Guimaraes and M. Cardozo, J. Chem. Inf. Model. **48** (5), 958 (2008).
40. J. L. Banks, H. S. Beard, Y. Cao, et al., J. Comput. Chem. **26** (16), 1752 (2005).
41. E. Polak and G. Ribiere, *ESAIM: Mathematical Modelling and Numerical Analysis—Modélisation Mathématique et Analyse Numérique* (1969), Vol. 3, p. 35.
42. X. Q. Xie and J. Z. Chen, J. Chem. Inf. Model. **48** (3), 465 (2008).
43. A. W. Schuttelkopf and D. M. van Aalten, Acta Crystallogr. D **60** (8), 1355 (2004).
44. R. A. Friesner, J. L. Banks, R. B. Murphy, et al., J. Med. Chem. **47** (7), 1739 (2004).
45. S. Van Der David, L. Erik, H. Berk, et al., J. Comput. Chem. **26** (16), 1701 (2005).
46. E. Krissinel and K. Henrick, J. Mol. Biol. **372** (3), 774 (2007).
47. A. A. Lashkov, S. E. Sotnichenko, I. I. Prokofiev, et al., Acta Crystallogr. D **68** (8), 968 (2012).
48. A. A. Lashkov, N. E. Zhukhlistova, A. H. Gabdoulkhakov, et al., Acta Crystallogr. D **66**, Part 1, 51 (2010).
49. M. G. Rossmann and P. Argos, Annu. Rev. Biochem. **50**, 497 (1981).
50. W. Bu, E. C. Settembre, M. H. Kouni, et al., Acta Crystallogr. D **61** (7), 863 (2005).
51. T. H. Tran, S. Christoffersen, P. W. Allan, et al., Biochemistry **50** (30), 6549 (2011).
52. T. Miyahara, H. Nakatsuji, and T. Wada, J. Phys. Chem. A **118** (16), 2931 (2014).
53. D. Cao, R. L. Russell, D. Zhang, et al., Cancer Res. **62** (8), 2313 (2002).
54. M. Iigo, K. Nishikata, and A. Hoshi, Jpn J. Cancer Res. **83** (4), 392 (1992).
55. C. J. van Groeningen, G. J. Peters, and H. M. Pinedo, Semin. Oncol. **19** (2), 148 (1992).

Translated by T. Safonova